

Review

Recent Progress on Ultrathin Metalenses for Flat Optics

Seong-Won Moon,^{1,3} Yeseul Kim,^{1,3} Gwanho Yoon,^{1,3} and Junsuk Rho^{1,2,*}

SUMMARY

As technology advances, electrical devices such as smartphones have become more and more compact, leading to a demand for the continuous miniaturization of optical components. Metalenses, ultrathin flat optical elements composed of metasurfaces consisting of arrays of subwavelength optical antennas, provide a method of meeting those requirements. Moreover, metalenses have many other distinctive advantages including aberration correction, active tunability, and semi-transparency, compared to their conventional refractive and diffractive counterparts. Therefore, over the last decade, great effort has been focused on developing metalenses to investigate and broaden the capabilities of metalenses for integration into future applications. Here, we discuss recent progress on metalenses including their basic design principles and notable characteristics such as aberration correction, tunability, and multifunctionality.

INTRODUCTION

Optical lenses are critical components in scientific technologies such as microscopy, display, and optical lithography. Conventional refractive lenses composed of transparent convex or concave materials are widely used but are bulky and limit the miniaturization of optical components. Moreover, complex and time-consuming three-dimensional (3D) surface machining is required to make aspherical refractive lenses for spherical aberration correction. Diffractive lenses with a sawtooth profile provide an alternative way to realize thin and compact lensing, but the focusing capability is inherently limited by the shadowing effect; diffractive lenses are available for low numerical aperture (NA) only (Lu et al., 2010; Banerji et al., 2019).

As an alternative, metasurfaces, two-dimensional arrays of subwavelength antennas (Yu and Capasso, 2014; Jeong et al., 2020), can be utilized as ultrathin optical devices. When light interacts with a metasurface, the transmitted and reflected waves can be arbitrarily modulated by engineering the physical shape of antennas (Yu et al., 2011). Many applications of metasurfaces have been demonstrated, including ultrathin lenses, holograms, and optical cloaks (Kim et al., 2018; Yoon et al., 2018, Yoon et al., 2019a, Yoon et al., 2019b; Rho, 2020; Lee et al., 2020b; Ren et al., 2020). Metalenses provide an opportunity to realize high-end ultrathin lenses without the limitations of the shadowing effect. Therefore, much effort has been devoted to developing metalenses.

In this review, we discuss recent progress on metalenses, including the working principles, material dependence, and fabrication methods. We will also discuss aberration correction and tunability, which are two distinct advantages of metalenses compared to conventional diffractive lenses. Finally, we will introduce the state-of-the-art applications of metalenses.

METALENS DESIGN

The basic goal of optical lens is to focus incident light at a target point. Metalenses are flat; each subwavelength-scale meta-atom on the metasurface acts as an antenna or a waveguide for a phase shift (Wang et al., 2017a). The points at a position (x, y) on a metalens require a different phase delay, as they are at different distances from the focal point. The spatial phase profile $\phi(x, y)$ must follow the following equation:

$$\phi(x, y) = \frac{2\pi}{\lambda} \left(\sqrt{x^2 + y^2 + f^2} - f \right) \quad (\text{Equation 1})$$

where λ is the wavelength and f is the focal length.

¹Department of Mechanical Engineering, Pohang University of Science and Technology, Pohang 37673, Republic of Korea

²Department of Chemical Engineering, Pohang University of Science and Technology, Pohang 37673, Republic of Korea

³These authors contributed equally

*Correspondence:
jshro@postech.ac.kr

<https://doi.org/10.1016/j.isci.2020.101877>



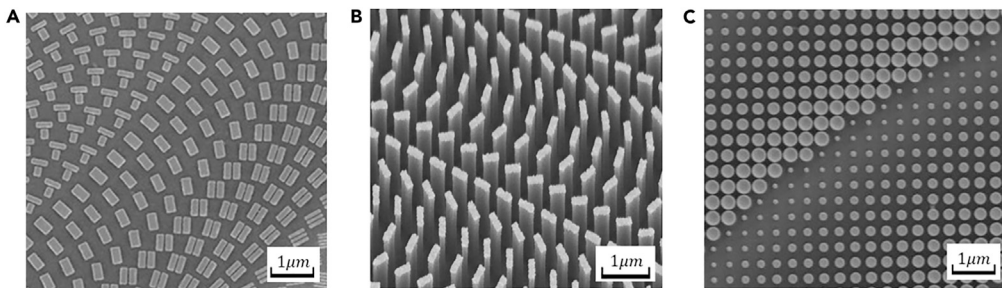


Figure 1. Scanning Electron Micrograph of Metalenses Classified by Phase Modulation Types

(A) Plasmonic resonant type metalens that compensates for phase by using controlled aspect ratio and two resonant wavelengths of gold nanorods. Reprinted with permission from (Wang et al., 2017b). Copyright 2017, Springer Nature.

(B) Geometric phase type of metalens in which phase shift is achieved by rotation of silicon nanofins by systematically increasing angles. Reprinted with permission from (Khorasaninejad et al., 2016a). Copyright 2016, American Chemical Society.

(C) Propagation phase type metalens in which the effective index is adjusted to reach the required phase profile by modifying the diameters of TiO_2 nanopillar according to the position. Reprinted with permission from (Khorasaninejad et al., 2016b). Copyright 2016, American Chemical Society.

Phase can be modulated by resonant effect, non-resonant effect, or by combination of both. Resonant strategies (Figure 1A) exploit excitations in response to incident radiation (Genevet et al., 2017; Wang et al., 2017b). These tuning effects include Mie resonance, Fabry-Pérot resonance (Anzan-Uz-Zaman et al., 2020), plasmonic resonance, and extended resonance in high-contrast arrays (Arbabi et al., 2015b). Resonant type metalenses operate in narrow bandwidth but benefit from high reproducibility and productivity due to their smaller aspect ratio than non-resonant types.

The non-resonant type metalenses exploit the modulation of geometric or propagation phase (Chen et al., 2020c). The former, also known as Pancharatnam-Berry (PB) phase, uses anisotropic nanofins that operate as a half-wave plate (Figure 1B) (Piccirillo et al., 2017; Yang et al., 2017; Khorasaninejad et al., 2016a). The nanofins in every uniform structural unit cell operate as subwavelength scatterers, so the wavefront is reshaped depending on the rotation of the meta-atom and the direction of polarization of the incident light because of the birefringent retardation effect (Yu and Capasso, 2014). The azimuthal rotation of meta-atoms to a certain angle θ contributes an amount of phase shift as follows:

$$\phi(x, y) = \pm 2\theta(x, y) \quad (\text{Equation 2})$$

The sign is determined by the direction of the circular polarization of the incident wave. The latter method is achieved by manipulating the diameter and height of the nanopillars and the lattice periodicity to adjust the effective refractive index of the unit cell (Figure 1C) (Bayati et al., 2019; Khorasaninejad et al., 2016b). In general cases, meta-atoms of propagation phase type are polarization insensitive and have a broader band of operating wavelengths than resonant metalenses (Zhan et al., 2016; Liang et al., 2019; Mahmood et al., 2018), but polarization-sensitive non-resonant type metalenses have been designed by combining both the geometric and the propagation phase methods (Yan et al., 2019; Rubin et al., 2019; Zhou et al., 2019).

The building materials of metalenses are selected according to their physical properties and the desired operating wavelength. Ideal materials for metalenses have a high refractive index and low absorption coefficient. Plasmonic materials have been widely used for metalenses in early research (Ni et al., 2013), but performance is hindered by high optical losses which prevent the efficiency from reaching over 25% (Chen et al., 2018a), so the focus has changed toward all-dielectric metasurfaces which can be designed to have the efficiency close to 90% (Genevet et al., 2017; West et al., 2014; Khorasaninejad et al., 2016b). In fact, high efficient metasurfaces which utilize all-metal or metal-dielectric-metal integrated structures have been developed as optical applications (Xie et al., 2019; Zheng et al., 2015); we can look on the bright possibility of improvement on plasmonic metalens. Recently, the mainstream of material choice is still dielectric, but improving efficiency of metalens by adopting complementary structure with both metallic and dielectric materials is also reported (Li et al., 2020a) because plasmonic metallic materials have advantages from

the view point of lower aspect ratio and high producibility in fabrication compared with the dielectric material (Liang et al., 2019)

Both refractive index and absorption coefficient vary with wavelength, so the most suitable dielectric material is determined by the wavelength range in which the lens is to be used (Liang et al., 2019). For example, germanium (Ge) and silicon (Si) are suitable for use in the infrared band (Wang et al., 2019, 2020a), titanium dioxide (TiO_2) and gallium nitride (GaN) are suitable for the visible band (Khorasaninejad et al., 2017a; Huang et al., 2020), and hafnium oxide (HfO_2) and aluminum nitride (AlN) are suitable for the UV band (Zhang et al., 2020a; Guo et al., 2018).

Development of large-area fabrication and mass production methods are key requirements to enable the practical use of metalenses as a replacement for conventional refractive lenses. Conventional methods such as electron beam lithography (EBL) and focused ion beam (FIB) milling have been widely used for metalens fabrication (Chen et al., 2019d; Verslegers et al., 2009), but they are time-consuming processes. Therefore, several alternative techniques have been developed. For example, the use of an electron beam resist has been used to simplify the lithography steps and reduce production time (Andrén et al., 2020), stepper projection by photolithography and deep UV (DUV) photolithography has enabled the rapid production of large-scale metalenses (She et al., 2018a; Park et al., 2019), and single-step UV nanoimprint lithography using a high-index nanocomposite has been demonstrated to allow rapid fabrication of high-efficiency metalenses with a single step of nanoimprinting without any secondary operations such as thin-film deposition or etching (Yoon et al., 2020).

Metalenses allow for the development of compact, efficient, and multifunctional optical systems or devices (Lu and Liu, 2012; Khorasaninejad and Capasso, 2017). Metalenses exploit metasurface optics and are therefore lighter, thinner, and more compact than refractive lenses. Consequently, metalenses have the potential to replace conventional optical components in integrated or microscale optics (Tseng et al., 2018). High-NA metalenses have been achieved by controlling various degrees of freedom (Liu et al., 2018a; Decker et al., 2019; Khorasaninejad et al., 2016c, 2017b). Structural and material optimization can yield metalenses that have near-unity NA (Kang et al., 2020; Kotlyar et al., 2019; Paniagua-Domínguez et al., 2018; Fan et al., 2018) or even $NA > 1$ (Liang et al., 2018; Huang et al., 2019); these overcome the limited NA of conventional diffractive lenses (Arbabi et al., 2015a; Engelberg and Levy, 2020; Meem et al., 2020). For example, metalenses with an ultra-high NA have been achieved using crystalline silicon nanostructures on sapphire substrates (Liang et al., 2018). The lenses have an $NA = 0.98$ in air and $NA = 1.48$ when operated in an immersion liquid. Efficient and high-NA metalenses can help to achieve diffraction-limited focusing and high-resolution imaging. Moreover, metalenses that have properties or functions that change under certain conditions have been reported (Mansouree et al., 2020; Shirmanesh et al., 2020; Xu et al., 2020). These multifunctional characteristics suggest the possibility that metalenses can be used in imaging, spectroscopy, 3D depth vision, and augmented reality.

ABERRATION CORRECTION

Correction of aberration is an important challenge in the design of optical lenses. Aberration makes light spread across a region of space rather than concentrate on a specific focal point and can be both monochromatic and achromatic. Compared to conventional refractive or diffractive lenses (Lalanne et al., 1999; Khorasaninejad et al., 2015; Lin et al., 2014), the physical working principles of metalenses are more diverse, so they present additional ways to rectify unwanted aberration. Metalenses even offer a way to solve both monochromatic and achromatic focusing problems simultaneously (Kim et al., 2020c; Arbabi et al., 2016a).

To prevent monochrome light from spreading around the point of focus, monochromatic aberration must be removed. This form of aberration has five causes: spherical aberration, coma, astigmatism, curvature of field, and distortion. A hyperbolic phase profile (Equation 1) removes spherical aberration at normal incidence. However, off-axis aberration enlarges as the incident angle increases; therefore, correction of aberration impedes development of high-NA lenses, which need a large field of view (FOV). Superposition of a sinusoidal phase profile on a hyperboloidal phase distribution can correct aberration under off-axis incidence (Kalvach and Szabó, 2016). Multilayer or doublet-structured metalenses also reduce monochromatic aberration correction under oblique incidence. An optical system that contains flat lens and curved aplastic metasurface patterned with nano-resonators eliminates coma and spherical aberration (Figure 2A) (Aieta et al., 2013). A doublet metalens in which one side of the metasurface works as an aperture lens

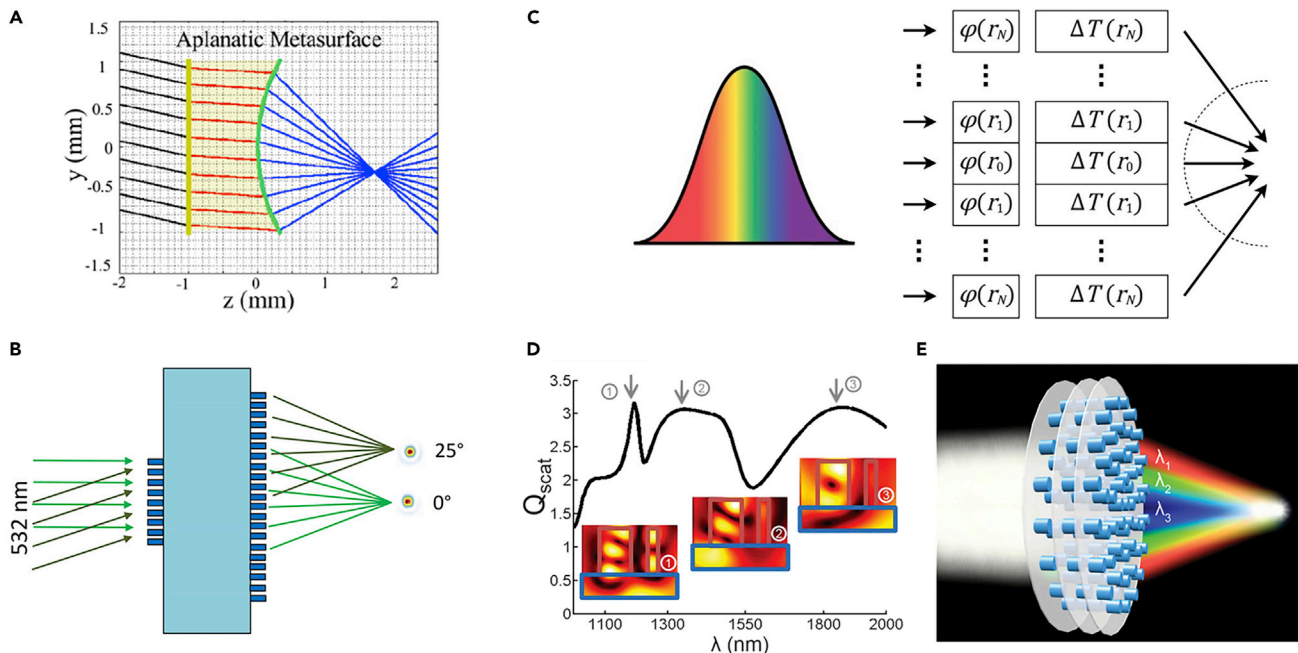


Figure 2. Aberration Corrected Metasurfaces

(A) Ray tracing plot for coma and spherical aberration-corrected optical system that uses metasurfaces. Reprinted with permission from (Aieta et al., 2013). Copyright 2013, The Optical Society.

(B) Monochromatic doublet metasurface that eliminates spherical aberration. Reprinted with permission from (Groever et al., 2017). Copyright 2017, American Chemical Society.

(C) Schematic view of focusing mechanism against time delay depending on wavelength. Reprinted with permission from (Presutti and Monticone, 2020). Copyright 2020, The Optical Society.

(D) Plot of scattering efficiency for one unit cell that shows peaks due to resonant and coupling effects between two dielectric resonators. Reprinted with permission from (Aieta et al., 2015). Copyright 2015, The American Association for the Advancement of Science.

(E) Multilayer metasurfaces for focusing multiple target wavelengths without chromatic aberration. Reprinted with permission from (Zhou et al., 2018). Copyright 2018, American Chemical Society.

and the other as a focusing lens has been shown to eliminate spherical aberration at $\lambda = 532$ nm (Figure 2B) (Groever et al., 2017). Correction of monochromatic aberration in metasurfaces must also improve focusing efficiency and maintain high NA (Aieta et al., 2012). Therefore, numerical or topological optimization has been used to increase the efficiency and correct multiple monochromatic aberration (Lin et al., 2018; Aieta et al., 2013; Arbabi et al., 2016b).

Correction of achromatic aberration is necessary for lenses that are intended to operate over a range of wavelengths. Critical physical properties such as transmittance, reflectance, and absorption rely on the wavelength of incident radiation. If the incident beam contains several wavelengths or a wide band of wavelengths, the tuning phase becomes cumbersome. To obtain achromatic aberration correction, the time to reach the focal point must be the same for all wavelengths (Figure 2C) (Presutti and Monticone, 2020). The frequency-dependent phase profile can be represented using a Taylor expansion as follows:

$$\phi(r, \omega) = \phi(r, \omega_t) + \left. \frac{\partial \phi(r, \omega)}{\partial \omega} \right|_{\omega=\omega_t} (\omega - \omega_t) + \left. \frac{\partial^2 \phi(r, \omega)}{\partial \omega^2} \right|_{\omega=\omega_t} (\omega - \omega_t)^2 + \dots \quad (\text{Equation 3})$$

where $\phi(r, \omega)$ is the phase at radial coordinate r with frequency ω and ω_t is the target frequency (Liang et al., 2019). The first term indicates the relative phase, which is affected by position and target frequency; the higher-order terms vary as the wavelength departs from the target wavelength. The second term represents the group delay; to prevent achromatic aberration, it must be independent of wavelength (Wang et al., 2017b). In that case, the group delay dispersion (third term) becomes imperceptible (Capasso, 2018). Unfortunately, at oblique incidence, additional phase compensation must be applied to control the off-axis dispersion in the polychromatic case (Dou et al., 2020). The amount of phase that must be

compensated for increases exponentially with distance away from the center. Therefore, the fabrication of a large-area achromatic metalens is a difficult task. As a response, inverse design methods have been exploited to achieve both large-scale and broad operating wavelengths (Lin et al., 2018).

Dispersive phase compensation can be achieved in several ways. Diverse methods to accomplish single-layer achromatic metasurfaces have been reported. Selecting the design of meta-atoms depends on a phase modulating mechanism which affects the phase and phase dispersion at each position (Shrestha et al., 2018; Chen et al., 2019d). Applying spatial multiplexing (Lin et al., 2016; Li et al., 2017; Arbabi et al., 2016c), cascading (McClung et al., 2020), or catenary (Pu et al., 2015; Zhang et al., 2020b), metasurfaces are widely used methods for achromatic focusing, and combining computational imaging with flat optics (Colburn et al., 2018) is also adopted for broadband phase modulating. Several metasurfaces that exploit resonance on dielectric (Aieta et al., 2015; Arbabi et al., 2017; Chen et al., 2018a, 2018c; Wang et al., 2018) or plasmonic (Hu et al., 2016; Wang et al., 2017a; Hsiao et al., 2018) meta-atoms have been demonstrated. One example using dielectric resonators shows that chromatic aberration of metasurfaces can be suppressed (Figure 2D); two asymmetrically designed building blocks introduce a broad resonance spectrum that eliminates the chromatic aberration (Aieta et al., 2015). Combining two or more phase modulating methods can also be utilized to make polarization-insensitive broadband achromatic metasurfaces (Chen et al., 2019d).

Multi-layer stacked metasurfaces can eliminate chromatic aberration. In multilayer metasurfaces, composed of amorphous silicon meta-atoms embedded in polydimethylsiloxane (PDMS), the operating wavelength range has been shown to broaden with an increase in the number of stacked layers (Figure 2E) (Zhou et al., 2018). A three-layer lens using disk-shaped metallic antennas to exploit localized surface plasmonic resonances of three different metallic components and achieve polarization-independent focusing in a broad range of visible light has also been demonstrated (Avayu et al., 2017). Because the thickness of each layer is tens of or hundreds of nanometer scale, the total thickness is only a few micrometers which means that multi-layer metasurfaces can be designed as ultrathin optical components.

TUNABLE FOCUSING

Tunability is a noteworthy feature of metasurfaces. In fact, designing tunable and reconfigurable metasurfaces has attracted great attention in flat optics, and various research studies have been reported (Kim et al., 2021; Nemati et al., 2018; Yu et al., 2018). The key point of tunable metasurfaces is that the meta-atoms that make up two-dimensional metasurfaces can be tuned under certain external stimuli to have a great potential to achieve dynamically configurable phase shift (Lee et al., 2020a; He et al., 2019). Several approaches to fabricate tunable or reconfigurable metasurfaces have been demonstrated. We classify the tunable metasurfaces according to three dominant modulating mechanisms, as (1) thermally, (2) electrically, and (3) mechanically tunable metasurfaces.

Thermal modulation of metasurfaces exploits the response to temperature by altering the complex refractive index, which affects the phase shift and its phase distribution (Iyer et al., 2018). One thermally tunable metasurface (Afridi et al., 2018) using a spiral gold heater to mediate an increase in temperature has demonstrated (Figure 3A); the refractive index varies depending on the thermal coefficient dn/dT as the temperature changes (Berto et al., 2019). This kind of tunable metasurface, which uses both electrically and thermally mediated phenomena, is classified as electro-thermo-optical systems.

Phase change materials have been used to construct optical devices that are thermally tunable in the visible or IR spectrum. Stimuli that induce the phase changes can include optical excitation and electrical current pulses, in addition to temperature change (Bai et al., 2019). One example is a phase-changed material-based writable device that is stimulated by optical excitation (Wang et al., 2016). Good thermal stability and speed of response to temperature have become key challenges in development of thermally tunable metasurfaces. Some phase change materials like GeSbTe (GST) and vanadium oxide (VO_2) have rapid switching speed and high stability, so they have been evaluated for use in these lenses (Loke et al., 2012; Bai et al., 2019). In bifocal metasurfaces, the focal distance increases when the phase of GST changes from amorphous to crystalline (Yin et al., 2017) as a result of a difference in the plasmonic resonances of the two phases (Figure 3B). A duplex focusing metasurface using VO_2 has been demonstrated as a transmission lens at room temperature due to its insulating property but switches into a reflective lens at 355 K, at which the VO_2 becomes metallic (Xu et al., 2020).

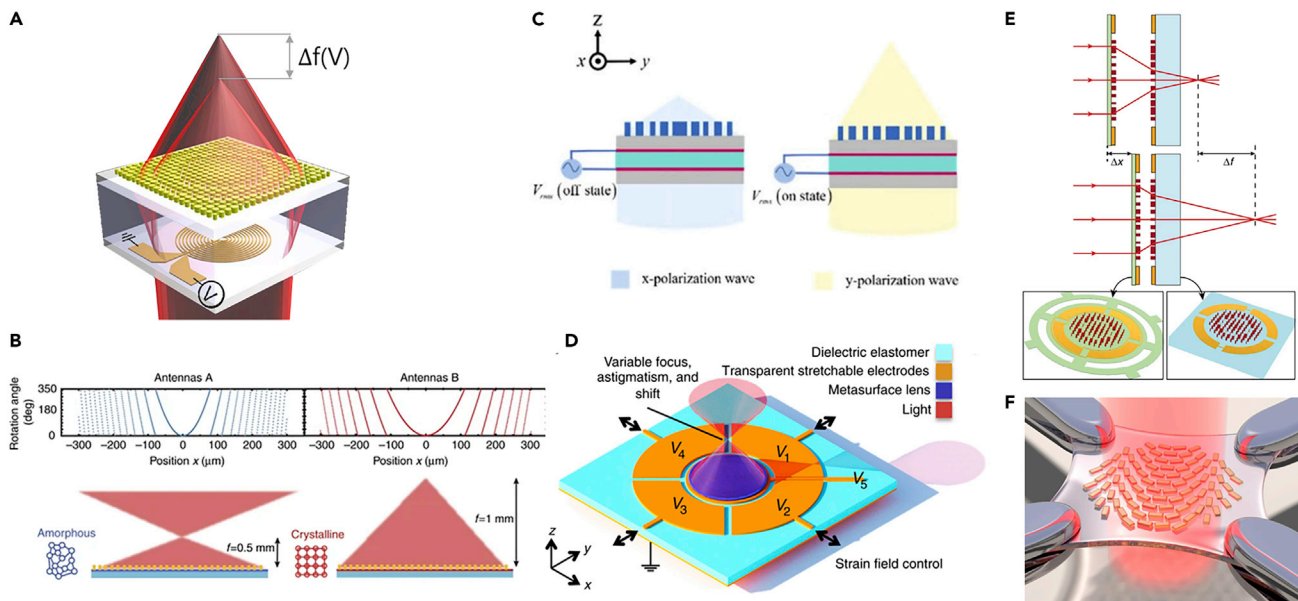


Figure 3. Tunable Metalenses

(A) Electro-thermo-optics-based varifocal metasurface which is integrated with a gold spiral heater. Reprinted with permission from (Afridi et al., 2018). Copyright 2018, American Chemical Society.

(B) Comparison of rotation angle and focusing profile of a bifocal cylindrical plasmonic metasurface. Its focal point depends on the states of the phase change material, GST. Reprinted with permission from (Yin et al., 2017). Copyright 2017, Springer Nature.

(C) Side views of electrically tuning metasurfaces integrated with a liquid crystal (LC) layer which changes the polarization direction of the incident beam. Reprinted with permission from (Fan et al., 2020a). Copyright 2020, The Optical Society.

(D) Schematic view of electrically tuning metasurfaces which controls strain field by applying electrical bias to artificial muscles. Reprinted with permission from (She et al., 2018b). Copyright 2018, The American Association for the Advancement of Science.

(E) MEMS metasurfaces that tune the location of the focal point by adjusting the distance between two metasurfaces. Reprinted with permission from (Arbabi et al., 2018a). Copyright 2018, Springer Nature.

(F) Schematic illustration of mechanically tuning a metasurface. The lattice constant of gold nanorod arrays depends on the stretch ratio of PDMS substrate, and the constant affects the focal length. Reprinted with permission from (Ee and Agarwal, 2016). Copyright 2016, American Chemical Society.

In electrically tunable metasurfaces, the phase shift is obtained using a biasing electrical voltage. Design of field-effect-induced tunable metasurfaces has exploited the increase in complex dielectric permittivity of meta-atoms in proportion to their carrier concentration (Thyagarajan et al., 2017). A metasurface with a tunable NA and focal length exploiting the change in carrier density in response to the application of an electric field has been presented (Shirmanesh et al., 2020); this lens has the advantages that the changes do not entail a change in form, and the tuning is faster than thermally tunable lenses. The use of a liquid crystal (LC) layer on a metasurface can enable instantaneous electrical control. In one such metasurface, the position of the focal point varies depending on the polarization of the incident wave that can be modulated by an electrical stimulus on the LC layer (Fan et al., 2020a); this system includes a layer of twisted nematic LCs that convert the polarization direction of the incident light when the electrical state is on or off (Figure 3C). The lens shows sub-millisecond response time and is compatible with complementary metal-oxide-semiconductor (CMOS) technology. Shen et al. (2020) have demonstrated a tunable achromatic metasurface with the inclusion of an LC layer. The focusing characteristics, whether achromatic or dispersive focusing, are determined by the saturated bias on the LC. Furthermore, introducing a strain-field-mediated metasurface can be another method for instantaneous electrical control. One example is a metasurface to which dielectric elastomer actuators are attached, then adjusted by varying the applied voltage to each electrode; as a result, the wavefront can be manipulated to control the astigmatism, focal length, and lateral shift (Figure 3D) (She et al., 2018b). The lens is only 30 μm thick, so it can be applied to compact optical devices for lateral control of magnification and correction of aberration.

Mechanical stimuli of an optical system can cause structural changes that affect the position, size, and shape of focal points. These stimuli include electrostatic actuating (Arbabi et al., 2018a), rotating (Cui et al., 2019; Guo et al., 2019; Wei et al., 2020), and stretching (Liu et al., 2018b; Cheng et al., 2019; Kamali

et al., 2016; Ee and Agarwal, 2016). In a double optical structure obtained using microelectromechanical systems, the focal length is controlled by regulating the distance between two metasurfaces (Figure 3E) (Arbabi et al., 2018a); a static layer is electrostatically connected to a movable layer, and the focal length decreases as the distance between the layers increases. This device has a high tuning speed and ultrathin structure so can be used in fast-scanning 3D imaging and endoscopy. Furthermore, adjusting mutual rotating angle of doublet metalenses or polarizer is one of the mechanically tuning methods. One proposed doublet metalens exploits the Moiré effect by combining two chiral geometric metasurfaces (Cui et al., 2019); the doublet metalens presents a positive focusing effect on left-circularly polarized (LCP) light or a negative effect on right-circularly polarized (RCP) light, so the focal point zooms continuously as the angle of rotation changes. Physical stretching of the four edges of a PDMS substrate achieves a continuous zoom effect (Figure 3F) (Ee and Agarwal, 2016). Stretching increases the distance between gold nanorods, so the shape and curvature of phase shift change.

IMAGING APPLICATIONS

A metalens can be used in tomography to enable non-destructive inspection. The endoscope for optical coherence tomography suffers from astigmatism and spherical aberration (Tearney et al., 1997; Gora et al., 2017). By replacing a conventional catheter with metalenses, the endoscope can achieve subdiffractive-limited imaging and extended depth of focus with negligible astigmatism (Figures 4A and 4B) (Pahlevaninezhad et al., 2018).

Recently, an aplanatic metalens-based spectral tomographic imaging system for high transverse and longitudinal resolution has been proposed (Chen et al., 2019a). The distance between the objective lens and the sample is quite short in microscopic imaging systems, so the visual field from the object approximates a spherical wave rather than a plane wave. In this reason, a hyperbolic metalens that is designed to process a plane wave causes a large spherical aberration in microscopic imaging. An aplanatic metalens designed for a spherical wave incidence can focus the objective field without spherical aberration and thereby achieve high resolution in both transverse and longitudinal directions.

The flatness of metalenses enables fabrication of compact systems. A combination of a flat metalens with a photonic crystal that works as a Laplacian operator has been developed for a monolithic compound imaging system (Zhou et al., 2020). It can conduct bright-field imaging at $\lambda = 1280$ nm and image differentiation at $\lambda = 1120$ nm (Figure 4C).

The metalenses detect depth information, in addition to imaging objects in the focal plane. Light-field imaging, which measures the intensity of the scene and direction of the light rays, has been widely used to reconstruct out-of-focus images and to obtain depth information of objects (Wilburn et al., 2005; Georgiev and Lumsdaine, 2010). However, for correct image rendering and depth detection, the chromatic and spherical aberration of optical components such as microlens arrays used in conventional light-field imaging systems must be solved. These problems can be overcome in the visible region by using an array of 60×60 achromatic metalenses that use GaN nanoantennas (Figure 4D) (Lin et al., 2019). The proposed light-field camera has great advantages of nearly diffraction-limited resolution for a white light source and compatibility with semiconductor processes. An achromatic metalens array that uses SiN nanoantennas achieved polarization-insensitive light-field imaging in the visible range (Fan et al., 2019). The geometries of nanoantennas that satisfy both nearly zero effective material dispersion and different effective refractive indexes are varied while the symmetry of the structures with a hole at the center was maintained.

Light-field imaging that uses metalenses can obtain highly resolved 3D information for single fluorescent particle tracking, which is an important technique in dynamic biology. Many researchers have tried to dynamically track single particles with a high lateral and axial resolution by using several methods such as deconvolution algorithms (Prevedel et al., 2014) and wavefront coding techniques (Shechtman et al., 2016). However, conventional methods to track fluorescent particles in 3D use microlens arrays that have limited NA of lenses in microlens arrays; these characteristics of the devices limit their ability to simultaneously satisfy high lateral resolution and high axial resolution. A light-field tracking system composed of a light-field metalens and a standard microscope can overcome the limited spatial resolution (Holsteen et al., 2019). The light-field metalens composed of three interleaved metalenses is placed on the specimen, so it provides lateral resolution finer than $0.8 \mu\text{m}$ and axial resolution finer than $73 \mu\text{m}$. The great benefits of

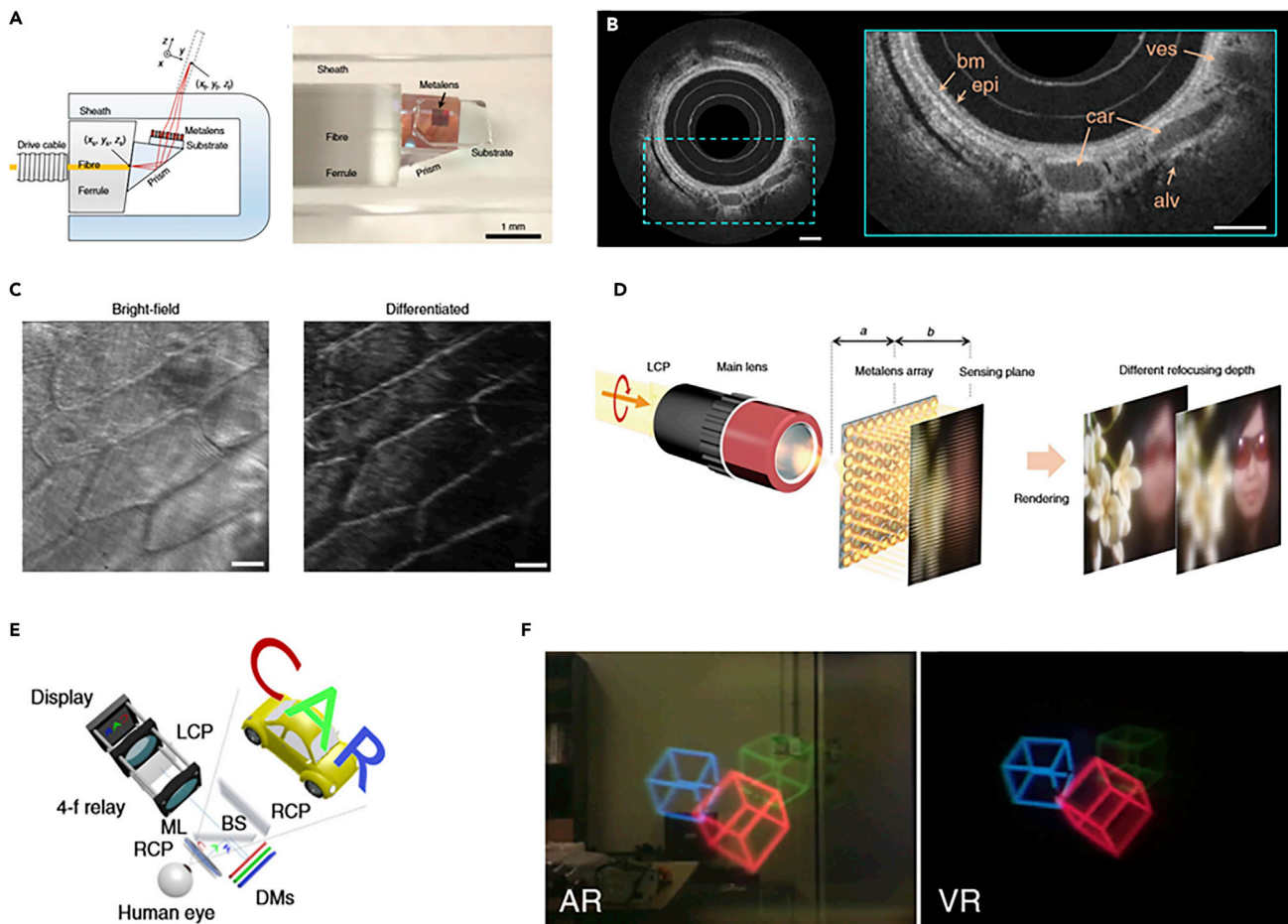


Figure 4. Chromatic and Achromatic Metalenses for Imaging

- (A) Schematic (left) and photography (right) of endoscopic optical coherence tomography system. The working distance of a metalens is 0.5 mm. Reprinted with permission from (Pahlevaninezhad et al., 2018). Copyright 2018, Springer Nature.
- (B) Tomography of *in vivo* the upper airways of sheep, as obtained by an endoscope that uses a metalens. Scale bars, 500 μ m. Reprinted with permission from (Pahlevaninezhad et al., 2018). Copyright 2018, Springer Nature.
- (C) Bright-field (left) and differentiated (right) images of onion cells at $\lambda = 1280$ nm and $\lambda = 1120$ nm. Scale bars, 50 μ m. Reprinted with permission from (Zhou et al., 2020). Copyright 2020, Springer Nature.
- (D) Schematic view of light-field imaging by using a 60×60 achromatic metalens array and rendered images of refocusing depth. Reprinted with permission from (Lin et al., 2019). Copyright 2019, Springer Nature.
- (E) Schematic of an augmented reality display system based on chromatic metalens eyepiece with a diameter of 20 mm and NA of 0.61. Reprinted with permission from (Lee et al., 2018). Copyright 2018, Springer Nature.
- (F) Realized images for augmented (left) and virtual (right) reality. Reprinted with permission from (Lee et al., 2018). Copyright 2018, Springer Nature.

particle tracking by light-field metalenses allow good resolution without the need to modify a standard microscope.

A metalens can provide a wide FOV to an imaging system. Double-layer metalenses for wide-angle imaging without spherical and coma aberration have introduced in the previous section. However, fabrication of multilayer metalenses requires a complex process, and the device has a thickness of hundreds of micrometers to millimeters. In contrast to metalenses, multilevel diffractive lenses for wide-angle imaging have been demonstrated, but they still suffer from coma aberration (Banerji et al., 2019). A single-layer metalens with micrometer thickness (Hao et al., 2020) can eliminate both spherical and coma aberration in the visible range. The metalens has a diameter of 1 mm and NA = 0.45 and had resolution finer than 2.2 μ m and FOV of 32° × 32°.

Type	Metalens Use	Resolution (nm)	Operation Wavelength (nm)	Ref
SIL-STED microscopy	No	2.4 ± 0.3	532, 775	Wildanger et al., 2012
Microsphere microscopy	No	23	White light	Chen et al. (2018b, 2019b)
Structured illumination microscopy	No	45	405, 488	Li et al., 2015
Superoscillation	Yes	0.264	800	Yuan et al. (2019)
Two-photon microscopy	Yes	930, 680	822, 600	Arbabi et al. (2018b)
Tomography	Yes	775	450–660	Chen et al. (2019a)
Light-field camera	Yes	1950	400–660	Lin et al. (2019)
Light-field particle tracking	Yes	800	600	Holsteen et al. (2019)

Table 1. Summary of Recent Optical Imaging System

SIL-STED, solid immersion lens-stimulated emission depletion.

The limited FOV impedes the use of metalenses in virtual and augmented reality. The conventional augmented reality systems suffer from the low FOV and NA of conventional optical elements and a large form factor. An eye-closed metalens, which is fabricated by nanoimprinting at a large diameter of 20 mm, had NA = 0.61; in experiments, it widened the FOV of the virtual and augmented reality system to as much as 90° (Figure 4E) (Lee et al., 2018). The virtual image is focused by the metalens, while ambient light just passes through it without interaction. The imaging capability for nonlinear imaging might be improved by using metalenses (Schlickriede et al., 2018, 2020).

To compare recent optical imaging performance, the resolutions of optical imaging techniques are summarized in Table 1. Note that the resolution is important in imaging but is not the absolute criterion of the performance of optical systems. For example, microsphere-enhanced optical imaging shows flexible and good optical properties with high resolution but requires to contact a microsphere to the surface of the sample or complex setup to use a non-contact mode (Chen et al., 2019b). Therefore, various aspects such as resolution, imaging time, and target object should be considered to evaluate the optical system. However, the performance of lens is directly connected to the resolution of imaging. This summary will help to improve optical imaging system using metalens.

MULTIFUNCTIONAL METALENSES

The multi-functionality of the metalens enables reduction in the size of optical elements and increase in the versatility of optical systems. A multifunctional metalens can be used to control the focus or the transmittance depending on fundamental characteristics of the incident light such as frequency and polarization (Arbabi et al., 2015a; Lin and Li, 2019; Faraji-Dana et al., 2018; Zhu et al., 2017). This section introduces various multifunctional metalenses that can operate differently at different frequencies or in several states of polarization.

A metalens can be designed to have different locations of focus for the different incident wavelengths or wavelength bands. Computer-generated holography (CGH) can be used to design a metalens that has a multi-focal spot in the co-plane. An iterative Fourier transform algorithm method based on Fresnel diffraction is used to calculate the phase profile of a multifocal metalens at $\lambda = 541, 621$, and 750 nm (Huang et al., 2020); the simulated full width at half maximum (FWHM) of focal spots showed that the metalens designed by CGH overcomes the optical diffraction limit $\lambda/(2 \times NA)$.

A metalens that focuses beams with different orbital angular momentum states at different wavelengths has also been reported (Shi et al., 2018). For example, the proposed reflective metalens simultaneously focuses the red and green light but generates a focused vortex beam for blue at the same focal distance. The advantages of wavelength-controlled metalens can support development of compact stimulated-emission-depletion microscopes (Vicidomini et al., 2018).

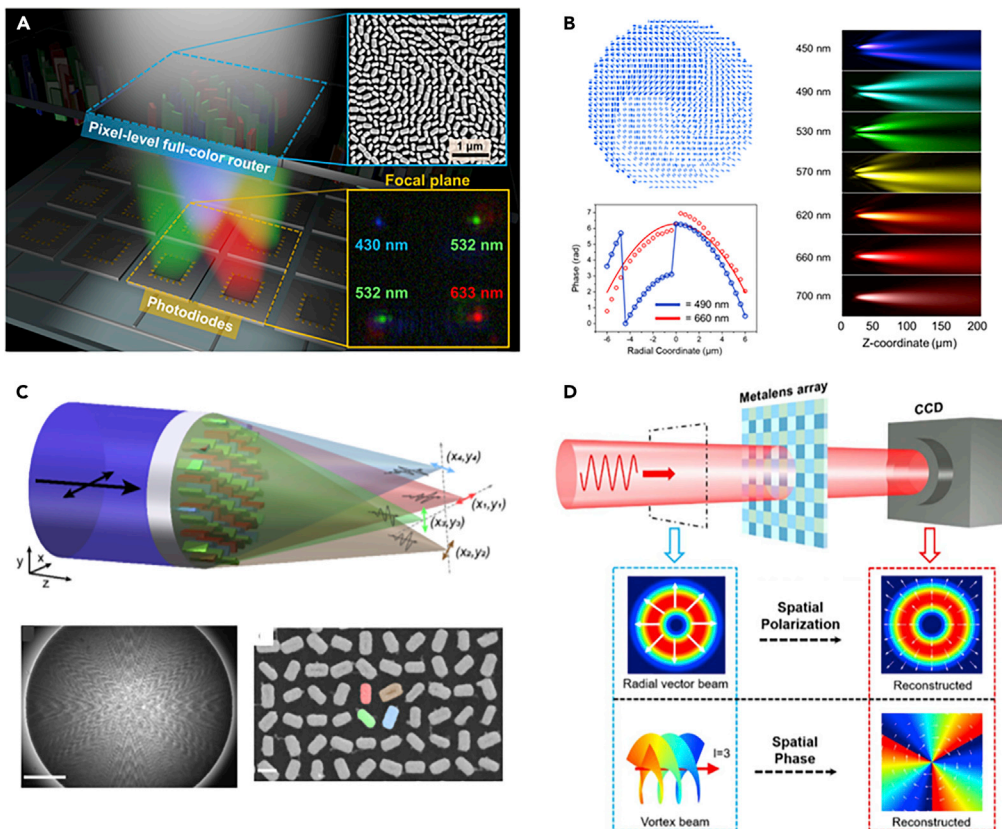


Figure 5. Frequency and Polarization Multifunctional Metalens-Based Devices

(A) Schematic of frequency-dependent metalens for separating focal spots of RGB components. Three frequency multiplexed unit cells consist of four nanopillars: one for red, two for green, and one for blue. Reprinted with permission from (Chen et al., 2017). Copyright 2017, American Chemical Society.

(B) Structure and focusing simulation of a multifunctional metasurface in two different bandwidths. The metasurface is designed for focusing donut-shaped light at 450–530 nm and focal spot at 620–700 nm by dispersion engineering. Reprinted with permission from (Sisler et al., 2020). Copyright 2020, American Institute of Physics.

(C) Schematic and SEM images of the metalens focusing at different positions in the focal plane for each linear polarization. Scale bars, (left) 20 μm and (right) 200 nm. Reprinted with permission from (Chen et al., 2020a). Copyright 2020, American Chemical Society.

(D) Schematic diagram of spatial polarized states and a phase profile detector with a metalens array. Six different polarization-dependent metalenses make up a sub-pixel in metalens array. Reprinted with permission from (Wang et al., 2020c). Copyright 2020, The Optical Society.

A wide range of research has considered multifunctional metalenses that are composed of a single structure in a unit cell. However, transmissive metalenses have limitations in improving frequency-dependent versatility because it is difficult to impart the required phases at each frequency with high efficiency in the broadband frequency range using a single structure. Therefore, unit cells composed of several structures have been used to obtain metalenses that can perform different functions at several frequencies. A full-color router was obtained by using metalenses that focus red, green, and blue at different spatial positions (Figure 5A) (Chen et al., 2017). The multiplex unit cell is composed of a 4×4 array of GaN nanopillars, with 1:2:1 ratio of nanopillars optimized for red, green, and blue transmission.

Meta-atoms composed of two nanopillars give metalenses a large number of degrees of freedom of optical properties related to frequency. This freedom provides the required phase and group delay to impart achromatic, refractive, and diffractive properties into a metalens that has dual focal length in different frequency ranges. Moreover, control of their dispersion can be used to independently design phase profiles for a donut-shaped focal spot at $450 \text{ nm} \leq \lambda \leq 530 \text{ nm}$ and an Airy disk at $450 \text{ nm} \leq \lambda \leq 700 \text{ nm}$ (Figure 5B) (Sisler et al., 2020).

Dispersion engineering using nanopillar pairs can also correct the aberration of an off-axis metalens. Especially, astigmatism and curvature of focal plane due to the chromatic aberration of grating and off-axis lens restrict the spectral resolution and bandwidth of conventional spectrometers. Additional optical components to compensate for these challenges increase the bulk and complexity of the system. A compact, aberration-corrected spectrometer has been achieved using a non-dispersive off-axis metalens (Zhu et al., 2019); implementation of the required phase, group delay, and group delay dispersion enables the proposed off-axis metalens to focus on the plane parallel to metalens plane, while maintaining invariant focal length for several wavelengths. The proposed spectrometer has a resolution of a nanometer on average, across a 200 nm spectral range in the visible.

The polarization state of the light is changed when it passes through an optical component (Saleh and Teich, 2019). The multifunction can be embedded in a metalens by exploiting the meta-atom's anisotropy. For example, by combining PB phase and propagation phase, a metalens can focus at different arbitrary positions for the orthogonally polarized incident light. High-efficiency metalenses that have dual or multiple focal lengths have been implemented by changing two circularly polarized states of incident light (Tian et al., 2019). The focal length is 10 μm under LCP light but 13 μm under RCP light. Under the x-polarized light, this metalens can separate the focus at longitudinally different positions. The x-polarized light can be decomposed into LCP and RCP, so each circularly polarized component contributes to an individual focus.

A trifocal metalens that focuses at three spots in different planes, depending on the input and output linearly polarized states, has been proposed (Gao et al., 2019b). Two types of meta-atoms are interleaved to yield a metalens that has three phase profiles. One independently modulates the phase of co-polarized light for two orthogonally linear polarized incident beams. Another converts the polarized state of the incident beam to cross-polarization with arbitrary phase delay. For example, when horizontally polarized light passes through the metalens, co- and cross-polarized components occur and each contribute to a different focus. Therefore, the metalens can generate two focuses for non-converted components of two orthogonally polarized light sources and one focus for converted components of the incident light. Another proposed metalens can continuously vary a focus by changing the state of polarization of the incident light from RCP to LCP (Zhang et al., 2019). The focal length can vary by 9.7 μm ; at $\lambda = 633 \text{ nm}$, the focusing efficiency is 63.1% for LCP and 59.9% for RCP.

Transverse location of focus can also be shifted by changing states of polarization. Off-axis metalens that focuses two circularly polarized light in each off-axis position has been reported (Groever et al., 2018). These functions are implemented by superposing polarization-independent quadratic phase and polarization-dependent linear phase. Circular polarization-dependent imaging with high focusing efficiency near 70% has been demonstrated.

For the case of a transverse multifocal metalens, a planar metalens to enable parallel illumination for polarization imaging has been reported (Figure 5C) (Chen et al., 2020a). A unit cell composed of four nanopillars allows the metalens to manipulate states of polarization and phase independently by combining the PB phase and the propagation phase.

The desired variability of a metalens includes more properties than focal length. Image zoom is another important property. Conventional zoom lenses use a mechanical strategy and entail a complex design, which are not applicable to flat lenses (Demenikov et al., 2009). A doublet metalens can tune the depth of focus in response to linear polarization of incident light (Fu et al., 2019). Under incident x-polarized light, the front metalens acts as a concave lens, whereas the rear metalens focuses the light; under y-polarized light, both metalenses operate as convex lenses. The design method yields a doublet metalens that can switch between short focal length mode and long focal length mode while maintaining the image plane; this ability allows step zooming without moving the object or the lens.

Control of spin states of incident light and distance between two metalens enables implementation of three functions (camera lens, compound microscope, and telescope) in one system (Yu et al., 2020). It uses different types of metalenses that have different polarization characteristics from each other. One metalens is composed of nanoposts and is polarization independent, and the other is composed of nano-fins and is polarization dependent. The phase of the former is determined by the nanoposts with different radii; the latter has PB phase that is achieved by appropriate tilting of nanofins. When the metalenses share

their focus and RCP light strikes them, both metalenses act as convex lenses; under these conditions, the metalens doublet can function as a camera lens. The separation distance between the two metalenses is smaller than the sum of their focal lengths, so a virtual image occurs and its magnification increases; under these conditions, the metalens doublet becomes a compound microscope. This principle is easily explained by the lens equation. In contrast, when the incident light is LCP, only the polarization-dependent metalens works as a concave lens; under these conditions, the doublet of concave and convex metalens operates as a simple telescope.

Polarization multifunctional metalens can also detect polarization. A dielectric metalens system composed of six different metalenses as sub-pixels can detect spatial polarization states and phase profile of incident beam ([Figure 5D](#)) ([Wang et al., 2020c](#)). The six different metalenses in each sub-pixel focus at distinct positions that correspond to the end of a Poincaré sphere's axis. The full Stokes parameters can be derived from the measured intensities of six focuses, and the states of spatial polarization can be calculated using the full Stokes parameters. The relative local phase and phase gradient can be calculated using the measured positions of focuses in a sub-pixel. The polarization multifunctionality of the metalens can also provide various opportunities for multiplexing deflection and focusing ([Gao et al., 2019a](#)) and for multi-generation of an optical vortex ([Wang et al., 2020b](#)). In addition to multifunctionality of polarization and frequency, angle multifunctional metalens gives miniaturized and powerful tools to quantitative phase imaging. Recently, the quantitative phase gradient microscopy composed of two cascaded angle multifunctional metalenses with a thickness of several millimeters has been reported ([Kwon et al., 2020](#)). Metalens at the first layer differently focuses the phase objects for transverse electric (TE) and transverse magnetic (TM) polarized light. Then, the field passing through the first metalens is separated into three different directions and propagates toward three metalenses at the second layer. Three metalenses, which have different phase offsets between TE and TM polarized light, provide differential interference contrast (DIC) images. The proposed compact microscopy can capture three DIC images in a single shot and acquire quantitative phase images through a computational process.

In one proposed design, dynamic modulation of focal length and intensity of a metalens can be achieved by varying the power of the incident beam ([Klopfen et al., 2020](#)). The design concentrates the nonlinear Kerr effect of silicon ([Leuthold et al., 2010](#)) to continuously vary the focal length over a range of 2.5 μm . To increase the high-quality resonance that this nonlinearity provides, periodic notches are patterned along a pair of nanograting; they cause guided-mode resonance, which induce strong field resonance and hence a high-quality factor.

METALENS-INTEGRATED OPTICAL SYSTEM

Photonic crystal fiber (PCF) is a well-known waveguide for long-distance optical communication with high transmission efficiency. However, to modify the characteristics of transmitted light such as amplitude, phase, polarization, and mode after they pass through the PCF, additional components are required. These disadvantages have been overcome by integrating a metalens onto the end facet of an optical fiber ([Figure 6A](#)) ([Yang et al., 2019](#)). The metalens focuses the transmitted light that is outcoupled at the core of the PCF.

The flatness of a metalens can be used as an optical tweezer to trap micron-sized particles by tightly focusing light. This trait could be integrated with a lab-on-a-chip device ([Figure 6B](#)) ([Tkachenko et al., 2018](#)). The optical tweezer is constructed using a microfluidic chamber placed on a reflective metalens. To realize 3D trapping of particles, the metalens is modified to eliminate the inner Fresnel zones. The resulting tool enabled 3D trapping of spherical polystyrene particles of 2- μm diameter.

A metalens that combines a hyperbolic lens and a nanoprinted display has been reported ([Chen et al., 2020b](#)). It controls the phase of transmitted light and also manipulates the reflection. The metalens can focus the transmitted light regardless of its polarization state. When the incident light reflects from the metalens, it shows the different reflective images under incident x-polarization and incident y-polarization ([Figure 6C](#)). Therefore, the metalens can provide focusing and also serve as a reflective display.

Recently, various metalenses have been reported for focusing the light at a subdiffraction limit, the Abbé diffraction limit is still difficult to overcome. To break the Abbé diffraction limit in far field, optical lenses using optical superoscillatory phenomena have been widely used in optical vortex generators,

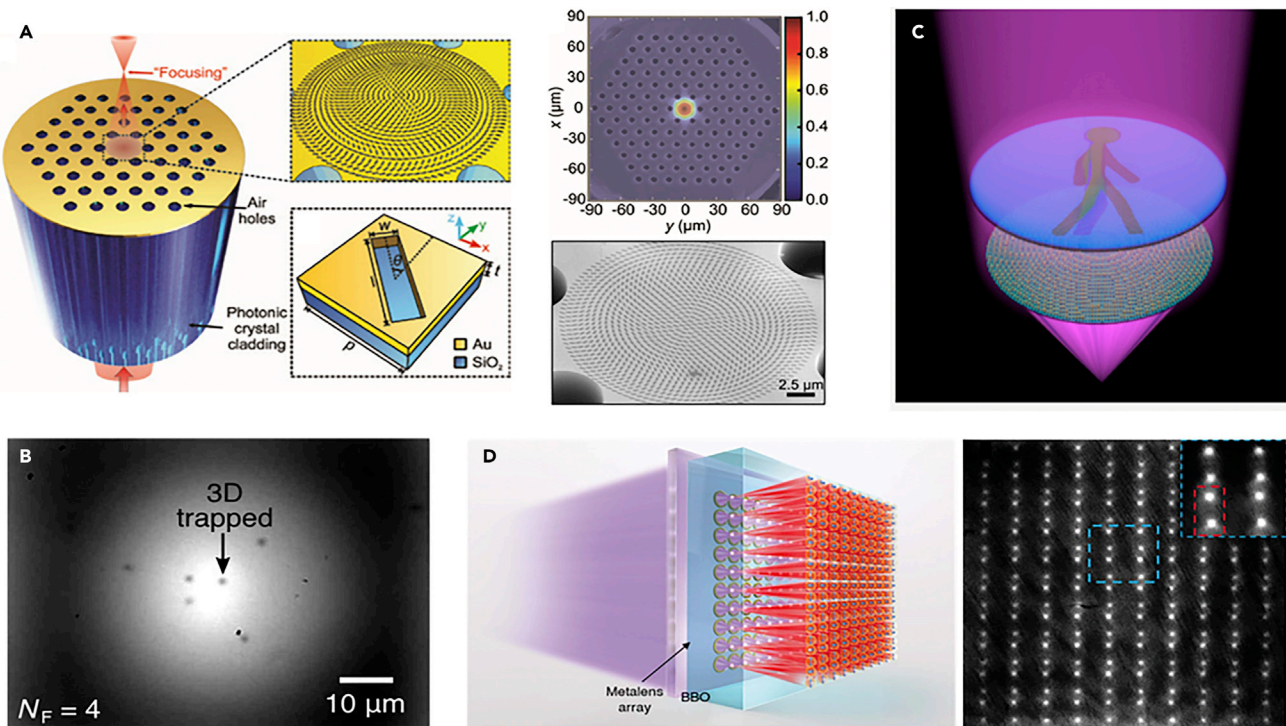


Figure 6. Optical Systems Combined with Metolenses

(A) PCF with plasmonic metolens fabricated at the end of the core. The schematic (left) of metolens-integrated PCF and unit cell of gold nanoslit. The SEM images (right): (upper) the end of the PCF superposing with single-mode simulation result and (lower) the metolens. Reprinted with permission from (Yang et al., 2019). Copyright 2019, De Gruyter.

(B) The experimental results of 3D trapping a single particle via a metolens-based optical tweezer. Reprinted with permission from (Tkachenko et al., 2018). Copyright 2018, The Optical Society.

(C) Schematic of metolens combining lens for transmitted light and nanoprinted display for reflected light. Reprinted with permission from (Chen et al., 2020b). Copyright 2020, American Chemical Society.

(D) Schematic of high-dimensional and multiphoton quantum source consisting of a metolens array. The individual metolens is designed with a focal length of 1 mm at $\lambda = 404$ nm wavelength and diameter 100 μm . The experimental result of spontaneous parametric downconversion photon pair array is shown in right of (D). Reprinted with permission from (Li et al., 2020b). Copyright 2020, The American Association for the Advancement of Science.

sub-wavelength microscopes, and super-resolution telescopes but suffer from narrow working frequency bandwidth (Berry et al., 2019). Broadband superoscillatory metolens that can focus beyond the Abbé diffraction limit in visible has been proposed (Tang et al., 2015, 2019). Another approach that uses vector diffractive optics has been also used to focus beyond the Abbé diffraction limit (Dorn et al., 2003). The key is to suppress the transverse electric field components of a radial vector beam to focus. The transverse components of radial vector beam focus in a ring shape, which spreads the focal spot. In contrast, the longitudinal electric field components contribute to focus on the optical axis, and the size of the focal spot is smaller than the size of a diffraction-limited spot. A metolens that converts linear polarized light to radially polarized light can focus the light beyond the Abbé diffraction limit and has been reported (Zuo et al., 2018). Appropriate elliptical nanoposts are selected to enable modulation of the states of spatial polarization and the required hyperbolic phase. Then, two additional design methods are applied to the metolens to restrict the contribution of transverse components to focus. One method is to place a circular aperture as a high-pass filter at the center of metolens; the other one is to add a radially extra phase like a radial grating effect. The focus of the device had FWHM = 0.386λ at $\lambda = 1105$ nm. A metolens may also enable artificial manipulation of the shapes of focus patterns (Ye et al., 2020).

The rapid development of metolenses has also affected quantum optics. Recently, high-dimensional two-photon path entanglement and generation of multiphoton state has been achieved by using a quantum source that uses a metolens array as a multiphoton quantum source (Figure 6D) (Li et al., 2020b). Each metolens has a diameter of 100 μm and a focal length of 1.1 mm at $\lambda = 404$ nm. This multiphoton quantum

Application	Material	Focusing Efficiency (%)	Operation Wavelength (nm)	Reference
Endoscope for OCT	a-Si	~80	1250–1370	Pahlevaninezhad et al. (2018)
Light-field camera	GaN	~39.1 ± 1.8	400–660	Lin et al. (2019)
Augmented reality	Poly-Si	12, 9, 2.5	660, 532, 473	Lee et al. (2018)
Color router	GaN	15.9, 38.33, 27.56	460, 532, 633	Chen et al. (2017)
Multiplexed orbital angular momentum metalens	TiO ₂	31, 37, 33	455, 540, 700	Shi et al. (2018)
Spectrometer	TiO ₂	~15	470–660	Zhu et al. (2019)
Varifocal metalens	GaN	59	633	Zhang et al. (2019)
Polarimeter	Si	48	1550	Wang et al. (2020c)
Quantitative phase gradient microscopy	a-Si	75	850	Kwon et al. (2020)
Photonic crystal fiber	Metal	16.4	1550	Yang et al. (2019)
Multiphoton quantum source	GaN	56 ± 6.6	404	Li et al. (2020b)

Table 2. Summary of Metalens-Application

OCT, optical coherence tomography.

source provides a compact device that is compatible with semiconductor processes and can contribute to the development of quantum optics.

In order to develop an optical system using metalens, characteristics of metalens such as target wavelength and focusing efficiency should be considered. From this point of view, we summarize materials, focusing efficiencies, and operating wavelengths of the representatives in Table 2. We believe that this summary will be helpful to study applications using metalens.

SUMMARY AND OUTLOOKS

The design principles and applications of metaleenses have been described, along with strategies of meta-atom design and the main materials used to construct lenses for use in the visible and near-infrared regimes. We have explained how metaleenses can overcome optical aberrations and categorized tunable metaleenses by the external stimulus of tuning focus. Finally, we have surveyed various metalens systems that have been applied to imaging, multifunctional devices, and integrated in other optical fields.

Although numerous novel and versatile metaleenses have been reported and applied to replace traditional bulk optical components in various fields, difficulties in modeling and fabrication are preventing the widespread adoption of metaleenses in the industry. In addition, many proposed optical systems using metalens has required additional optical components to filter unmodulated signal; the entire systems become bulk and suffer from low focusing efficiency. Therefore, polarization-independent and broadband achromatic metaleenses must be large and have both high NA and efficiency to realize compact optical systems that have no chromatic aberration. Recently, broadband and polarization-insensitive metalens composed of fishnet-like meta-atoms have shown high measured efficiencies of over 70% from the visible to the infrared regime (Nda et al., 2020). Furthermore, the development of aberration-free optical systems requires research to find ways to simultaneously correct chromatic and monochromatic aberration.

To facilitate the design and manufacture of metaleenses, electromagnetic simulation methods such as rigorous coupled-wave analysis, finite element method, and finite-difference time-domain methods are used to create libraries of meta-atoms in parametric form, so the computational costs increase with the complexity of the structure. For this reason, structures are kept simple which limits the possible degrees of freedom in the design. Inverse design methods, including machine learning and topology optimization, allow metasurfaces to overcome the limitations of degrees of freedom (Chen et al., 2019c; So et al., 2020;

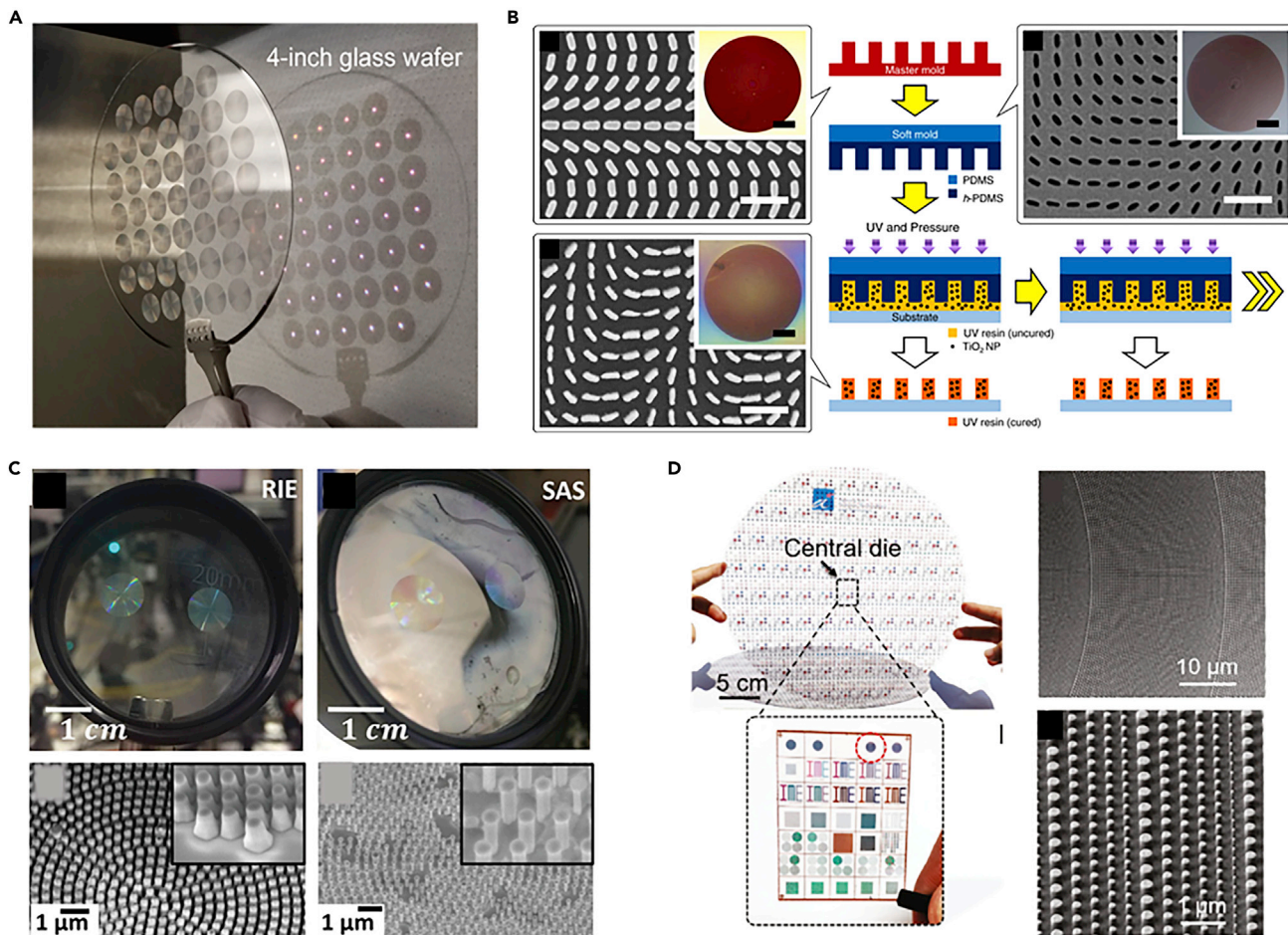


Figure 7. Large-Scale Manufacturing of Metalenses

(A) Metalens array fabricated by using DUV lithography on a 4-inch glass wafer. Reprinted with permission from (Park et al., 2019). Copyright 2019, American Chemical Society.

(B) Fabrication schematic of the nanoparticle composite-based scalable one-step printing process. Scale bars, 1 μm. (insets) Optical micrographs of each. Scale bars, 100 μm. Reprinted with permission from (Yoon et al., 2020). Copyright 2020, Springer Nature.

(C) Comparison of metalens fabrication results using conventional reactive ion etching (RIE) and selective area sublimation (SAS) on a sapphire wafer. Reprinted with permission from (Brière et al., 2019). Copyright 2019, John Wiley & Sons.

(D) (left) Metalenses fabricated by using DUV lithography on a 12-inch glass wafer. (right) SEM images of the metalens. Reprinted with permission from (Hu et al., 2020). Copyright 2020, De Gruyter.

Fan, 2020b). Furthermore, topology optimization methods combined with machine learning would be innovative approaches for the optimization of freeform metalens and metasurface (Jiang et al., 2019).

Materials that have a high refractive index and low optical loss should be identified. They would allow for a decrease in the aspect ratio of the meta-atoms and an increase in the focusing efficiency. Moreover, the degree of freedom of the metalenses may be increased by using meta-units that have several levels of height. Although multi-level diffractive lenses have been demonstrated, metalenses are currently limited to few levels of height.

Mass production of metalenses for commercialization requires the development of fabrication technologies that have lower cost and larger scale than EBL. A few low-cost, large-area metalenses have been manufactured using deep ultraviolet projection lithography (Figure 7A) (Park et al., 2019), but this method has insufficient patterning resolution compared with conventional EBL. Cascade domino lithography enables super-resolution patterning with sub-nanometer scale but not suitable to fabricate high-contrast metalens (Kim et al., 2020a, 2020b). Nanoimprint techniques can also provide a low-cost, large scale to fabricate metalenses. Recently, a scalable one-step printing method involving nanoparticle composite has been

proposed, and high-efficiency metalenses have been successfully demonstrated (Figure 7B) (Kim et al., 2019; Yoon et al., 2020, 2021). To realize a large-area metalens composed of dielectric materials, a novel non-etching fabrication method that combines nanoimprint with a selective area sublimation technique has been also proposed (Figure 7C) (Brière et al., 2019). However, nanoimprint methods limit the available materials and are difficult to precisely fabricate to produce a metalens. Metalenses fabricated by a CMOS-compatible process on a 12-inch glass wafer have also been reported (Hu et al., 2020), but they work in the near-infrared regime (Figure 7D). 3D laser direct writing techniques using femtosecond laser can also become an alternative to EBL and FIB (Serien and Sugioka, 2018; Saha et al., 2019). This high-throughput fabrication method not only manufactures large area in a short time compared to EBL or FIB but also patterns complex 3D structures with nanoscale. However, their low resolution and the limitation of available materials hinder applying to fabrication of metalens that focuses the visible light. Therefore, scalable, high-throughput, and elaborate manufacturing techniques are required for the mass production of metalenses at visible frequencies (Lee et al., 2020c).

Nevertheless, metalenses have strong advantages over conventional lenses, including their thin profile, low weight, diffraction-limited focusing, high NA, and unprecedented functions that cannot be achieved using other optical components. In addition, metalenses may be combined with other technologies to produce ultrahigh density organic light-emitting diodes (Joo et al., 2020), light detecting and ranging (Park et al., 2020; Xie et al., 2020), wearable optical devices, cameras for smartphones, and super-resolution microscopes. These properties represent the incredible potential of metalenses to lead optical engineering of the future with unprecedented applications in the future of optics.

Resource Availability

Lead Contact

Further information and requests for resources should be directed to and will be fulfilled by the Lead Contact, J. Rho (jsrho@postech.ac.kr).

Material Availability

Not Applicable.

Data and Code Availability

Not Applicable.

ACKNOWLEDGMENTS

This work was financially supported by the National Research Foundation (NRF) grants (NRF-2019R1A2C3003129, CAMM-2019M3A6B3030637, NRF-2019R1A5A8080290), funded by the Ministry of Science and ICT (MSIT) of the Korean government. Y.K. acknowledges a fellowship from Hyundai Motor Chung Mong-Koo Foundation. G.Y. acknowledges the NRF fellowship (NRF-2020R1A6A3A01097965) funded by the MSIT of the Korean government.

AUTHOR CONTRIBUTIONS

J.R. conceived the idea and initiated the project. S.-W.M., Y.K., and G.Y. wrote the manuscript. S.-W.M. and Y.K. prepared the figures. G.Y. outlined the manuscript. All authors read and provided feedback on the manuscript. J.R. guided the entire work.

REFERENCES

- Afridi, A., Canet-Ferrer, J., Philippet, L., Osmond, J., Berto, P., and Quidant, R. (2018). Electrically driven varifocal silicon metasens. *ACS Photon.* 5, 4497–4503.
- Aieta, F., Genevet, P., Kats, M.A., Yu, N., Blanchard, R., Gaburro, Z., and Capasso, F. (2012). Aberration-free ultrathin flat lenses and axicons at telecom wavelengths based on plasmonic metasurfaces. *Nano Lett.* 12, 4932–4936.
- Aieta, F., Genevet, P., Kats, M., and Capasso, F. (2013). Aberrations of flat lenses and aplanatic metasurfaces. *Opt. Express* 21, 31530–31539.
- Aieta, F., Kats, M.A., Genevet, P., and Capasso, F. (2015). Multiwavelength achromatic metasurfaces by dispersive phase compensation. *Science* 347, 1342–1345.
- Andrén, D., Martínez-Llinàs, J., Tassin, P., Käll, M., and Verre, R. (2020). Large-scale metasurfaces made by an exposed resist. *ACS Photon.* 7, 885–892.
- Anzan-Uz-Zaman, M., Song, K., Lee, D.-G., and Hur, S. (2020). A novel approach to Fabry-Pérot-resonance-based lens and demonstrating deep-subwavelength imaging. *Sci. Rep.* 10, 10769.
- Arbabi, A., Horie, Y., Bagheri, M., and Faraon, A. (2015a). Dielectric metasurfaces for complete control of phase and polarization with

subwavelength spatial resolution and high transmission. *Nat. Nanotechnol.* 10, 937–943.

Arbabi, A., Horie, Y., Ball, A.J., Bagheri, M., and Faraon, A. (2015b). Subwavelength-thick lenses with high numerical apertures and large efficiency based on high-contrast transmitarrays. *Nat. Commun.* 6, 7069.

Arbabi, A., Arbabi, E., Kamali, S.M., Horie, Y., Han, S., and Faraon, A. (2016a). Miniature optical planar camera based on a wide-angle metasurface doublet corrected for monochromatic aberrations. *Nat. Commun.* 7, 13682.

Arbabi, E., Arbabi, A., Kamali, S.M., Horie, Y., and Faraon, A. (2016b). Multiwavelength metasurfaces through spatial multiplexing. *Sci. Rep.* 6, 32803.

Arbabi, E., Arbabi, A., Kamali, S.M., Horie, Y., and Faraon, A. (2016c). Multiwavelength polarization-insensitive lenses based on dielectric metasurfaces with meta-molecules. *Optica* 3, 628–633.

Arbabi, E., Arbabi, A., Kamali, S.M., Horie, Y., and Faraon, A. (2017). Controlling the sign of chromatic dispersion in diffractive optics with dielectric metasurfaces. *Optica* 4, 625–632.

Arbabi, E., Arbabi, A., Kamali, S.M., Horie, Y., Faraji-Dana, M., and Faraon, A. (2018a). MEMS-tunable dielectric metasurface lens. *Nat. Commun.* 9, 812.

Arbabi, E., Li, J., Hutchins, R.J., Kamali, S.M., Arbabi, A., Horie, Y., Van Dorpe, P., Gradinaru, V., Wagenaar, D.A., and Faraon, A. (2018b). Two-photon microscopy with a double-wavelength metasurface objective lens. *Nano Lett.* 18, 4943–4948.

Avayu, O., Almeida, E., Prior, Y., and Ellenbogen, T. (2017). Composite functional metasurfaces for multispectral achromatic optics. *Nat. Commun.* 8, 14992.

Bai, W., Yang, P., Wang, S., Huang, J., Chen, D., Zhang, Z., Yang, J., and Xu, B. (2019). Actively tunable metasurface array based on patterned phase change materials. *Appl. Sci.* 9, 4927.

Banerji, S., Meem, M., Majumder, A., Vasquez, F.G., Sensale-Rodriguez, B., and Menon, R. (2019). Imaging with flat optics: metasurfaces or diffractive lenses? *Optica* 6, 805–810.

Bayati, E., Zhan, A., Colburn, S., Zhelyeznyakov, M.V., and Majumdar, A. (2019). Role of refractive index in metasurface performance. *Appl. Opt.* 58, 1460–1466.

Berry, M., Zheludev, N., Aharonov, Y., Colombo, F., Sabadini, I., Struppa, D.C., Tollaksen, J., Rogers, E.T.F., Qin, F., Hong, M., et al. (2019). Roadmap on superoscillations. *J. Opt.* 21, 053002.

Berto, P., Philippet, L., Osmond, J., Liu, C.F., Afridi, A., Montagut Marques, M., Molero Agudo, B., Tessier, G., and Quidant, R. (2019). Tunable and free-form planar optics. *Nat. Photon.* 13, 649–656.

Brière, G., Ni, P., Héron, S., Chenot, S., Vézian, S., Brändli, V., Damilano, B., Duboz, J.-Y., Iwanaga, M., and Genevet, P. (2019). An etching-free

approach toward large-scale light-emitting metasurfaces. *Adv. Opt. Mater.* 7, 1801271.

Capasso, F. (2018). The future and promise of flat optics: a personal perspective. *Nanophotonics* 7, 953–957.

Chen, B.H., Wu, P.C., Su, V.-C., Lai, Y.-C., Chu, C.H., Lee, I.C., Chen, J.-W., Chen, Y.H., Lan, Y.-C., Kuan, C.-H., et al. (2017). GaN metasurface for pixel-level full-color routing at visible light. *Nano Lett.* 17, 6345–6352.

Chen, C., Song, W., Chen, J.-W., Wang, J.-H., Chen, Y.H., Xu, B., Chen, M.-K., Li, H., Fang, B., Chen, J., et al. (2019a). Spectral tomographic imaging with aplanatic metasurface. *Light Sci. Appl.* 8, 99.

Chen, C., Wang, Y., Jiang, M., Wang, J., Guan, J., Zhang, B., Wang, L., Lin, J., and Jin, P. (2020a). Parallel polarization illumination with a multifocal axicon metasurface for improved polarization imaging. *Nano Lett.* 20, 5428–5434.

Chen, J., Zhang, F., Li, Q., Wu, J., and Wu, L. (2018a). A high-efficiency dual-wavelength achromatic metasurface based on panchromatic phase manipulation. *Opt. Express* 26, 34919–34927.

Chen, L., Zhou, Y., Wu, M., and Hong, M. (2018b). Remote-mode microsphere nano-imaging: new boundaries for optical microscopes. *Opto Electron. Adv.* 1, 170001.

Chen, L., Zhou, Y., Li, Y., and Hong, M. (2019b). Microsphere enhanced optical imaging and patterning: from physics to applications. *Appl. Phys. Rev.* 6, 021304.

Chen, L., Yin, Y., Li, Y., and Hong, M. (2019c). Multifunctional inverse sensing by spatial distribution characterization of scattering photons. *Opto Electron. Adv.* 2, 190019.

Chen, R., Zhou, Y., Chen, W., Chen, R., Iqbal, N., and Ma, Y. (2020b). Multifunctional metasurface: coplanar embedded design for metasurface and nanoprinted display. *ACS Photon.* 7, 1171–1177.

Chen, W.T., Zhu, A.Y., Sanjeev, V., Khorasaninejad, M., Shi, Z., Lee, E., and Capasso, F. (2018c). A broadband achromatic metasurface for focusing and imaging in the visible. *Nat. Nanotechnol.* 13, 220–226.

Chen, W.T., Zhu, A.Y., Sisler, J., Bharwani, Z., and Capasso, F. (2019d). A broadband achromatic polarization-insensitive metasurface consisting of anisotropic nanostructures. *Nat. Commun.* 10, 355.

Chen, W.T., Zhu, A.Y., and Capasso, F. (2020c). Flat optics with dispersion-engineered metasurfaces. *Nat. Rev. Mater.* 5, 604–620.

Cheng, F., Qiu, L., Nikolov, D., Bauer, A., Rolland, J.P., and Vamivakas, A.N. (2019). Mechanically tunable focusing metasurface in the visible. *Opt. Express* 27, 15194–15204.

Colburn, S., Zhan, A., and Majumdar, A. (2018). Metasurface optics for full-color computational imaging. *Sci. Adv.* 4, eaar2114.

Cui, Y., Zheng, G., Zheng, G., Chen, M., Zhang, Y., Yang, Y., Tao, J., He, T., Li, Z., and Li, Z. (2019).

Reconfigurable continuous-zoom metasurface in visible band. *Chin. Opt. Lett.* 17, 111603.

Decker, M., Chen, W.T., Nobis, T., Zhu, A.Y., Khorasaninejad, M., Bharwani, Z., Capasso, F., and Petschelt, J. (2019). Imaging performance of polarization-insensitive metasurfaces. *ACS Photon.* 6, 1493–1499.

Demenikov, M., Findlay, E., and Harvey, A.R. (2009). Miniaturization of zoom lenses with a single moving element. *Opt. Express* 17, 6118–6127.

Dorn, R., Quabis, S., and Leuchs, G. (2003). Sharper focus for a radially polarized light beam. *Phys. Rev. Lett.* 91, 233901.

Dou, K., Xie, X., Pu, M., Li, X., Ma, X., Wang, C., and Luo, X. (2020). Off-axis multi-wavelength dispersion controlling metasurface for multi-color imaging. *Opto Electron. Adv.* 3, 190005.

Ee, H.-S., and Agarwal, R. (2016). Tunable metasurface and flat optical zoom lens on a stretchable substrate. *Nano Lett.* 16, 2818–2823.

Engelberg, J., and Levy, U. (2020). The advantages of metasurfaces over diffractive lenses. *Nat. Commun.* 11, 1991.

Fan, C.-Y., Fan, C.-Y., Chuang, T.-J., Wu, K.-H., Su, G.-D.J., and Su, G.-D.J. (2020a). Electrically modulated varifocal metasurface combined with twisted nematic liquid crystals. *Opt. Express* 28, 10609–10617.

Fan, J.A. (2020b). Freeform metasurface design based on topology optimization. *MRS Bull.* 45, 196–201.

Fan, Z.-B., Shao, Z.-K., Xie, M.-Y., Pang, X.-N., Ruan, W.-S., Zhao, F.-L., Chen, Y.-J., Yu, S.-Y., and Dong, J.-W. (2018). Silicon nitride metasurfaces for close-to-one numerical aperture and wide-angle visible imaging. *Phys. Rev. Appl.* 10, 014005.

Fan, Z.-B., Qiu, H.-Y., Zhang, H.-L., Pang, X.-N., Zhou, L.-D., Liu, L., Ren, H., Wang, Q.-H., and Dong, J.-W. (2019). A broadband achromatic metasurface array for integral imaging in the visible. *Light Sci. Appl.* 8, 67.

Faraji-Dana, M., Arbabi, E., Arbabi, A., Kamali, S.M., Kwon, H., and Faraon, A. (2018). Compact folded metasurface spectrometer. *Nat. Commun.* 9, 4196.

Fu, R., Li, Z., Zheng, G., Chen, M., Yang, Y., Tao, J., Wu, L., and Deng, Q. (2019). Reconfigurable step-zoom metasurfaces without optical and mechanical compensations. *Opt. Express* 27, 12221–12230.

Gao, S., Park, C.-S., Lee, S.-S., and Choi, D.-Y. (2019a). A highly efficient bifunctional dielectric metasurface enabling polarization-tuned focusing and deflection for visible light. *Adv. Opt. Mater.* 7, 1801337.

Gao, S., Park, C.-S., Zhou, C., Lee, S.-S., and Choi, D.-Y. (2019b). Twofold polarization-selective all-dielectric trifocal metasurfaces for linearly polarized visible light. *Adv. Opt. Mater.* 7, 1900883.

Genet, P., Capasso, F., Aieta, F., Khorasaninejad, M., and Devlin, R. (2017). Recent advances in planar optics: from plasmonic to dielectric metasurfaces. *Optica* 4, 139–152.

- Georgiev, T., and Lumsdaine, A. (2010). Reducing plenoptic camera artifacts. *Comput. Graph. Forum* 29, 1955–1968.
- Gora, M.J., Suter, M.J., Tearney, G.J., and Li, X. (2017). Endoscopic optical coherence tomography: technologies and clinical applications [invited]. *Biomed. Opt. Express* 8, 2405–2444.
- Groever, B., Chen, W.T., and Capasso, F. (2017). Meta-lens doublet in the visible region. *Nano Lett.* 17, 4902–4907.
- Groever, B., Rubin, N.A., Mueller, J.P.B., Devlin, R.C., and Capasso, F. (2018). High-efficiency chiral meta-lens. *Sci. Rep.* 8, 7240.
- Guo, L., Hu, Z., Wan, R., Long, L., Li, T., Yan, J., Lin, Y., Zhang, L., Zhu, W., and Wang, L. (2018). Design of aluminum nitride metalens for broadband ultraviolet incidence routing. *Nanophotonics* 8, 171–180.
- Guo, Y., Pu, M., Ma, X., Li, X., Shi, R., and Luo, X. (2019). Experimental demonstration of a continuous varifocal metalens with large zoom range and high imaging resolution. *Appl. Phys. Lett.* 115, 163103.
- Hao, C., Gao, S., Ruan, Q., Feng, Y., Li, Y., Yang, J.K.W., Li, Z., and Qiu, C.-W. (2020). Single-layer aberration-compensated flat lens for robust wide-angle imaging. *Laser Photon. Rev.* 14, 2000017.
- He, Q., Sun, S., and Zhou, L. (2019). Tunable/reconfigurable metasurfaces: physics and applications. *Research* 2019, 1849272.
- Holsteen, A.L., Lin, D., Kauvar, I., Wetzstein, G., and Brongersma, M.L. (2019). A light-field metasurface for high-resolution single-particle tracking. *Nano Lett.* 19, 2267–2271.
- Hsiao, H.-H., Chen, Y.H., Lin, R.J., Wu, P.C., Wang, S., Chen, B.H., and Tsai, D.P. (2018). Integrated resonant unit of metasurfaces for broadband efficiency and phase manipulation. *Adv. Opt. Mater.* 6, 1800031.
- Hu, J., Liu, C.-H., Ren, X., Lauhon, L.J., and Odom, T.W. (2016). Plasmonic lattice lenses for multiwavelength achromatic focusing. *ACS Nano* 10, 10275–10282.
- Hu, T., Zhong, Q., Li, N., Dong, Y., Xu, Z., Fu, Y.H., Li, D., Bliznetsov, V., Zhou, Y., Lai, K.H., et al. (2020). CMOS-compatible a-Si metalenses on a 12-inch glass wafer for fingerprint imaging. *Nanophotonics* 9, 823–830.
- Huang, B., Bai, W., Jia, H., Han, J., Guo, P., Wu, J., and Yang, J. (2020). Multifocal co-plane metalens based on computer-generated holography for multiple visible wavelengths. *Results Phys.* 17, 103085.
- Huang, T.-Y., Grote, R.R., Mann, S.A., Hopper, D.A., Exarhos, A.L., Lopez, G.G., Kaighn, G.R., Garnett, E.C., and Bassett, L.C. (2019). A monolithic immersion metalens for imaging solid-state quantum emitters. *Nat. Commun.* 10, 2392.
- Iyer, P.P., DeCrescent, R.A., Lewi, T., Antonellis, N., and Schuller, J.A. (2018). Uniform thermo-optic tunability of dielectric metalenses. *Phys. Rev. Appl.* 10, 044029.
- Jeong, H., Yang, Y., Cho, H., Badloe, T., Kim, I., Ma, R.-M., and Rho, J. (2020). Emerging advanced metasurfaces: alternatives to conventional bulk optical devices. *Microelectron. Eng.* 220, 111146.
- Jiang, J., Sell, D., Hoyer, S., Hickey, J., Yang, J., and Fan, J.A. (2019). Free-form diffractive Metagrating design based on generative adversarial networks. *ACS Nano* 13, 8872–8878.
- Joo, W.-J., Kyoung, J., Esfandyarpour, M., Lee, S.-H., Koo, H., Song, S., Kwon, Y.-N., Song, S.H., Bae, J.C., Jo, A., et al. (2020). Metasurface-driven OLED displays beyond 10,000 pixels per inch. *Science* 370, 459–463.
- Kalvach, A., and Szabó, Z. (2016). Aberration-free flat lens design for a wide range of incident angles. *J. Opt. Soc. Am. B* 33, A66–A71.
- Kamali, S.M., Arbabi, E., Arbabi, A., Horie, Y., and Faraon, A. (2016). Highly tunable elastic dielectric metasurface lenses. *Laser Photon. Rev.* 10, 1002–1008.
- Kang, M., Ra'di, Y., Farfan, D., and Alù, A. (2020). Efficient focusing with large numerical aperture using a hybrid metalens. *Phys. Rev. Appl.* 13, 044016.
- Khorasaninejad, M., and Capasso, F. (2017). Metalenses: versatile multifunctional photonic components. *Science* 358, eaam8100.
- Khorasaninejad, M., Aieta, F., Kanhaiya, P., Kats, M.A., Genevet, P., Rousse, D., and Capasso, F. (2015). Achromatic metasurface lens at telecommunication wavelengths. *Nano Lett.* 15, 5358–5362.
- Khorasaninejad, M., Chen, W.T., Oh, J., and Capasso, F. (2016a). Super-dispersive off-axis meta-lenses for compact high resolution spectroscopy. *Nano Lett.* 16, 3732–3737.
- Khorasaninejad, M., Zhu, A.Y., Roques-Carmes, C., Chen, W.T., Oh, J., Mishra, I., Devlin, R.C., and Capasso, F. (2016b). Polarization-insensitive metalenses at visible wavelengths. *Nano Lett.* 16, 7229–7234.
- Khorasaninejad, M., Chen, W.T., Devlin, R.C., Oh, J., Zhu, A.Y., and Capasso, F. (2016c). Metalenses at visible wavelengths: diffraction-limited focusing and subwavelength resolution imaging. *Science* 352, 1190–1194.
- Khorasaninejad, M., Shi, Z., Zhu, A.Y., Chen, W.T., Sanjeev, V., Zaidi, A., and Capasso, F. (2017a). Achromatic metalens over 60 nm bandwidth in the visible and metalens with reverse chromatic dispersion. *Nano Lett.* 17, 1819–1824.
- Khorasaninejad, M., Chen, W.T., Zhu, A.Y., Oh, J., Devlin, R.C., Roques-Carmes, C., Mishra, I., and Capasso, F. (2017b). Visible wavelength planar metalenses based on titanium dioxide. *IEEE J. Sel. Top. Quan. Electron.* 23, 43–58.
- Kim, I., Yoon, G., Jang, J., Genevet, P., Nam, K.T., and Rho, J. (2018). Outfitting next generation displays with optical metasurfaces. *ACS Photon.* 5, 3876–3895.
- Kim, I., Mun, J., Hwang, W., Yang, Y., and Rho, J. (2020a). Capillary-force-induced collapse lithography for controlled plasmonic nanogap structures. *Microsyst. Nanoeng.* 6, 65.
- Kim, I., Mun, J., Baek, K.M., Kim, M., Hao, C., Qiu, C.-W., Jung, Y.S., and Rho, J. (2020b). Cascade domino lithography for extreme photon squeezing. *Mater. Today* 39, 89–97.
- Kim, I., Ansari, M.A., Mehmood, M.Q., Kim, W.-S., Jang, J., Zubair, M., Kim, Y.-K., and Rho, J. (2021). Stimuli-responsive dynamic metaholographic displays with designer liquid crystal modulators. *Adv. Mater.* 33, 2004664.
- Kim, K., Yoon, G., Baek, S., Rho, J., and Lee, H. (2019). Facile nanocasting of dielectric metasurfaces with sub-100 nm resolution. *ACS Appl. Mater. Interfaces* 11, 26109–26115.
- Kim, C., Kim, S.-J., and Lee, B. (2020c). Doublet metalens design for high numerical aperture and simultaneous correction of chromatic and monochromatic aberrations. *Opt. Express* 28, 18059–18076.
- Klopfer, E., Lawrence, M., Barton, D.R., Dixon, J., and Dionne, J.A. (2020). Dynamic focusing with high-quality-factor metalenses. *Nano Lett.* 20, 5127–5132.
- Kotlyar, V.V., Stafeev, S.S., Nalimov, A.G., and O'Faolain, L. (2019). Subwavelength grating-based spiral metalens for tight focusing of laser light. *Appl. Phys. Lett.* 114, 141107.
- Kwon, H., Arbabi, E., Kamali, S.M., Faraji-Dana, M., and Faraon, A. (2020). Single-shot quantitative phase gradient microscopy using a system of multifunctional metasurfaces. *Nat. Photon.* 14, 109–114.
- Lalanne, P., Astilean, S., Chavel, P., Cambril, E., and Launois, H. (1999). Design and fabrication of blazed binary diffractive elements with sampling periods smaller than the structural cutoff. *J. Opt. Soc. Am. A* 16, 1143–1156.
- Lee, G.-Y., Hong, J.-Y., Hwang, S., Moon, S., Kang, H., Jeon, S., Kim, H., Jeong, J.-H., and Lee, B. (2018). Metasurface eyepiece for augmented reality. *Nat. Commun.* 9, 4562.
- Lee, C.-W., Choi, H.J., and Jeong, H. (2020a). Tunable metasurfaces for visible and SWIR applications. *Nano Convergence* 7, 3.
- Lee, D., Gwak, J., Badloe, T., Palomba, S., and Rho, J. (2020b). Metasurfaces-based imaging and applications: from miniaturized optical components to functional imaging platforms. *Nanoscale Adv.* 2, 605–625.
- Lee, T., Lee, C., Oh, D.K., Badloe, T., Ok, J.G., and Rho, J. (2020c). Scalable and high-throughput top-down manufacturing of optical metasurfaces. *Sensors* 20, 4108.
- Leuthold, J., Koos, C., and Freude, W. (2010). Nonlinear silicon photonics. *Nat. Photon.* 4, 535–544.
- Li, D., Shao, L., Chen, B.-C., Zhang, X., Zhang, M., Moses, B., Milkie, D.E., Beach, J.R., Hammer, J.A., Pasham, M., et al. (2015). Extended-resolution structured illumination imaging of endocytic and cytoskeletal dynamics. *Science* 349, aab3500.
- Li, H., Fang, B., Chen, C., Zhu, S., and Li, T. (2020a). Cavity-enhanced metallic metalens with improved efficiency. *Sci. Rep.* 10, 417.

- Li, K., Guo, Y., Pu, M., Li, X., Ma, X., Zhao, Z., and Luo, X. (2017). Dispersion controlling meta-lens at visible frequency. *Opt. Express* 25, 21419–21427.
- Li, L., Liu, Z., Ren, X., Wang, S., Su, V.-C., Chen, M.-K., Chu, C.H., Kuo, H.Y., Liu, B., Zang, W., et al. (2020b). Metalens-array-based high-dimensional and multiphoton quantum source. *Science* 368, 1487–1490.
- Liang, H., Lin, Q., Xie, X., Sun, Q., Wang, Y., Zhou, L., Liu, L., Yu, X., Zhou, J., Krauss, T.F., et al. (2018). Ultrahigh numerical aperture metalens at visible wavelengths. *Nano Lett.* 18, 4460–4466.
- Liang, H., Martins, A., Borges, B.-H.V., Zhou, J., Martins, E.R., Li, J., and Krauss, T.F. (2019). High performance metalenses: numerical aperture, aberrations, chromaticity, and trade-offs. *Optica* 6, 1461–1470.
- Lin, R., and Li, X. (2019). Multifocal metalens based on multilayer Pancharatnam–Berry phase elements architecture. *Opt. Lett.* 44, 2819–2822.
- Lin, D., Fan, P., Hasman, E., and Brongersma, M.L. (2014). Dielectric gradient metasurface optical elements. *Science* 345, 298–302.
- Lin, D., Holsteen, A.L., Maguid, E., Wetzstein, G., Kik, P.G., Hasman, E., and Brongersma, M.L. (2016). Photonic multitasking interleaved Si nanoantenna phased array. *Nano Lett.* 16, 7671–7676.
- Lin, R.J., Su, V.-C., Wang, S., Chen, M.K., Chung, T.L., Chen, Y.H., Kuo, H.Y., Chen, J.-W., Chen, J., Huang, Y.-T., et al. (2019). Achromatic metalens array for full-colour light-field imaging. *Nat. Nanotechnol.* 14, 227–231.
- Lin, Z., Groever, B., Capasso, F., Rodriguez, A.W., and Lončar, M. (2018). Topology-optimized multilayered metaoptics. *Phys. Rev. Appl.* 9, 044030.
- Liu, C.-H., Zheng, J., Colburn, S., Fryett, T.K., Chen, Y., Xu, X., and Majumdar, A. (2018a). Ultrathin van der Waals metalenses. *Nano Lett.* 18, 6961–6966.
- Liu, W., Li, Z., Cheng, H., Tang, C., Li, J., Zhang, S., Chen, S., and Tian, J. (2018b). Metasurface enabled wide-angle Fourier lens. *Adv. Mater.* 30, 1706368.
- Loke, D., Lee, T.H., Wang, W.J., Shi, L.P., Zhao, R., Yeo, Y.C., Chong, T.C., and Elliott, S.R. (2012). Breaking the speed limits of phase-change memory. *Science* 336, 1566–1569.
- Lu, D., and Liu, Z. (2012). Hyperlenses and metalenses for far-field super-resolution imaging. *Nat. Commun.* 3, 1205.
- Lu, F., Sedgwick, F.G., Karagodsky, V., Chase, C., and Chang-Hasnain, C.J. (2010). Planar high-numerical-aperture low-loss focusing reflectors and lenses using subwavelength high contrast gratings. *Opt. Express* 18, 12606–12614.
- Mahmood, N., Kim, I., Mehmood, M.Q., Jeong, H., Akbar, A., Lee, D., Saleem, M., Zubair, M., Anwar, M.S., Tahir, F.A., et al. (2018). Polarisation insensitive multifunctional metasurfaces based on all-dielectric nanowaveguides. *Nanoscale* 10, 18323–18330.
- Mansouree, M., Kwon, H., Arbabi, E., McClung, A., Faraon, A., and Arbabi, A. (2020). Multifunctional 2.5D metastructures enabled by adjoint optimization. *Optica* 7, 77–84.
- McClung, A., Mansouree, M., and Arbabi, A. (2020). At-will chromatic dispersion by prescribing light trajectories with cascaded metasurfaces. *Light Sci. Appl.* 9, 93.
- Meem, M., Banerji, S., Pies, C., Oberbiermann, T., Majumder, A., Sensale-Rodriguez, B., and Menon, R. (2020). Large-area, high-numerical-aperture multi-level diffractive lens via inverse design. *Optica* 7, 252–253.
- Nda, A., Hsu, L., Ha, J., Park, J.-H., Chang-Hasnain, C., and Kanté, B. (2020). Octave bandwidth photonic fishnet-achromatic-metalens. *Nat. Commun.* 11, 3205.
- Nemati, A., Wang, Q., Hong, M., and Teng, J. (2018). Tunable and reconfigurable metasurfaces and metadevices. *Opto Electron. Adv.* 1, 180009.
- Ni, X., Ishii, S., Kildishev, A.V., and Shalaev, V.M. (2013). Ultra-thin, planar, Babinet-inverted plasmonic metalenses. *Light Sci. Appl.* 2, e72.
- Pahlevaninezhad, H., Khorasaninejad, M., Huang, Y.-W., Shi, Z., Hariri, L.P., Adams, D.C., Ding, V., Zhu, A., Qiu, C.-W., Capasso, F., et al. (2018). Nano-optic endoscope for high-resolution optical coherence tomography *in vivo*. *Nat. Photon.* 12, 540–547.
- Paniagua-Domínguez, R., Yu, Y.F., Khaidarov, E., Choi, S., Leong, V., Bakker, R.M., Liang, X., Fu, Y.H., Valuckas, V., Krivitsky, L.A., et al. (2018). A metalens with a near-unity numerical aperture. *Nano Lett.* 18, 2124–2132.
- Park, J., Jeong, B.G., Kim, S.I., Lee, D., Kim, J., Shin, C., Lee, C.B., Otsuka, T., Kyong, J., Kim, S., et al. (2020). All-solid-state spatial light modulator with independent phase and amplitude control for three-dimensional LiDAR applications. *Nat. Nanotechnol.* <https://doi.org/10.1038/s41565-020-00787-y>.
- Park, J.-S., Zhang, S., She, A., Chen, W.T., Lin, P., Yousef, K.M.A., Cheng, J.-X., and Capasso, F. (2019). All-glass, large metalens at visible wavelength using deep-ultraviolet projection lithography. *Nano Lett.* 19, 8673–8682.
- Piccirillo, B., Picardi, M.F., Marrucci, L., and Santamato, E. (2017). Flat polarization-controlled cylindrical lens based on the Pancharatnam–Berry geometric phase. *Eur. J. Phys.* 38, 034007.
- Presutti, F., and Monticone, F. (2020). Focusing on bandwidth: achromatic metalens limits. *Optica* 7, 624–631.
- Prevedel, R., Yoon, Y.-G., Hoffmann, M., Pak, N., Wetzstein, G., Kato, S., Schrödel, T., Raskar, R., Zimmer, M., Boyden, E.S., and Vaziri, A. (2014). Simultaneous whole-animal 3D imaging of neuronal activity using light-field microscopy. *Nat. Methods* 11, 727–730.
- Pu, M., Li, X., Ma, X., Wang, Y., Zhao, Z., Wang, C., Hu, C., Gao, P., Huang, C., Ren, H., et al. (2015). Catenary optics for achromatic generation of perfect optical angular momentum. *Sci. Adv.* 1, e1500396.
- Ren, H., Fang, X., Jang, J., Bürger, J., Rho, J., and Maier, S.A. (2020). Complex-amplitude metasurface-based orbital angular momentum holography in momentum space. *Nat. Nanotechnol.* 15, 948–955.
- Rho, J. (2020). Metasurfaces: subwavelength nanostructure arrays for ultrathin flat optics and photonics. *MRS Bull.* 45, 180–187.
- Rubin, N.A., D'Aversa, G., Chevalier, P., Shi, Z., Chen, W.T., and Capasso, F. (2019). Matrix fourier optics enables a compact full-Stokes polarization camera. *Science* 365, eaax1839.
- Saha, S.K., Wang, D., Nguyen, V.H., Chang, Y., Oakdale, J.S., and Chen, S.-C. (2019). Scalable submicrometer additive manufacturing. *Science* 366, 105–109.
- Saleh, B.E.A., and Teich, M.C. (2019). *Fundamentals of Photonics* (John Wiley & Sons).
- Serien, D., and Sugioka, K. (2018). Fabrication of three-dimensional proteinaceous micro- and nano-structures by femtosecond laser cross-linking. *Opto Electron. Adv.* 1, 180008.
- Schlückriede, C., Waterman, N., Reineke, B., Georgi, P., Li, G., Zhang, S., and Zentgraf, T. (2018). Imaging through nonlinear metalens using second harmonic generation. *Adv. Mater.* 30, 1703843.
- Schlückriede, C., Kruk, S.S., Wang, L., Sain, B., Kivshar, Y., and Zentgraf, T. (2020). Nonlinear imaging with all-dielectric metasurfaces. *Nano Lett.* 20, 4370–4376.
- She, A., Zhang, S., Shian, S., Clarke, D.R., and Capasso, F. (2018a). Adaptive metalenses with simultaneous electrical control of focal length, astigmatism, and shift. *Sci. Adv.* 4, eaap9957.
- She, A., Zhang, S., Shian, S., Clarke, D.R., and Capasso, F. (2018b). Large area metalenses: design, characterization, and mass manufacturing. *Opt. Express* 26, 1573–1585.
- Shechtman, Y., Weiss, L.E., Backer, A.S., Lee, M.Y., and Moerner, W.E. (2016). Multicolour localization microscopy by point-spread-function engineering. *Nat. Photon.* 10, 590–594.
- Shen, Z., Zhou, S., Li, X., Ge, S., Chen, P., Hu, W., and Lu, Y. (2020). Liquid crystal integrated metalens with tunable chromatic aberration. *Adv. Photon.* 2, 036002.
- Shi, Z., Khorasaninejad, M., Huang, Y.-W., Roques-Carmes, C., Zhu, A.Y., Chen, W.T., Sanjeev, Y., Ding, Z.-W., Tamagnone, M., Chaudhary, K., et al. (2018). Single-layer metasurface with controllable multiwavelength functions. *Nano Lett.* 18, 2420–2427.
- Shiranesh, G.K., Sokhoyan, R., Wu, P.C., and Atwater, H.A. (2020). Electro-optically tunable multifunctional metasurfaces. *ACS Nano* 14, 6912–6920.
- Shrestha, S., Overvig, A.C., Lu, M., Stein, A., and Yu, N. (2018). Broadband achromatic dielectric metasurfaces. *Light Sci. Appl.* 7, 85.
- Sisler, J., Chen, W.T., Zhu, A.Y., and Capasso, F. (2020). Controlling dispersion in multifunctional metasurfaces. *APL Photon.* 5, 056107.

- So, S., Badloe, T., Noh, J., Bravo-Abad, J., and Rho, J. (2020). Deep learning enabled inverse design in nanophotonics. *Nanophotonics* 9, 1041–1057.
- Tang, D., Wang, C., Zhao, Z., Wang, Y., Pu, M., Li, X., Gao, P., and Luo, X. (2015). Ultrabroadband superoscillatory lens composed by plasmonic metasurfaces for subdiffraction light focusing. *Laser Photon. Rev.* 9, 713–719.
- Tang, D., Chen, L., and Liu, J. (2019). Visible achromatic super-oscillatory metasurfaces for sub-diffraction focusing. *Opt. Express* 27, 12308–12316.
- Tearney, G.J., Brezinski, M.E., Bouma, B.E., Boppart, S.A., Pitris, C., Southern, J.F., and Fujimoto, J.G. (1997). In vivo endoscopic optical biopsy with optical coherence tomography. *Science* 276, 2037–2039.
- Thyagarajan, K., Sokhoyan, R., Zornberg, L., and Atwater, H.A. (2017). Millivolt modulation of plasmonic metasurface optical response via ionic conductance. *Adv. Mater.* 29, 1701044.
- Tian, S., Guo, H., Hu, J., and Zhuang, S. (2019). Dielectric longitudinal bifocal metalens with adjustable intensity and high focusing efficiency. *Opt. Express* 27, 680–688.
- Tkachenko, G., Stellinga, D., Ruskuc, A., Chen, M., Dholakia, K., and Krauss, T.F. (2018). Optical trapping with planar silicon metalenses. *Opt. Lett.* 43, 3224–3227.
- Tseng, M.L., Hsiao, H.-H., Chu, C.H., Chen, M.K., Sun, G., Liu, A.-Q., and Tsai, D.P. (2018). Metalenses: advances and applications. *Adv. Opt. Mater.* 6, 1800554.
- Verslegers, L., Catrysse, P.B., Yu, Z., White, J.S., Barnard, E.S., Brongersma, M.L., and Fan, S. (2009). Planar lenses based on nanoscale slit arrays in a metallic film. *Nano Lett.* 9, 235–238.
- Vicidomini, G., Bianchini, P., and Diaspro, A. (2018). STED super-resolved microscopy. *Nat. Methods* 15, 173–182.
- Wang, A., Chen, Z., and Dan, Y. (2019). Planar metalenses in the mid-infrared. *AIP Adv.* 9, 085327.
- Wang, Q., Rogers, E.T.F., Gholipour, B., Wang, C.-M., Yuan, G., Teng, J., and Zheludev, N.I. (2016). Optically reconfigurable metasurfaces and photonic devices based on phase change materials. *Nat. Photon.* 10, 60–65.
- Wang, S., Lai, J., Wu, T., Li, X., and Sun, J. (2017a). Wide-band achromatic metalens for visible light by dispersion compensation method. *J. Phys. D Appl. Phys.* 50, 455101.
- Wang, S., Wu, P.C., Su, V.-C., Lai, Y.-C., Hung Chu, C., Chen, J.-W., Lu, S.-H., Chen, J., Xu, B., Kuan, C.-H., et al. (2017b). Broadband achromatic optical metasurface devices. *Nat. Commun.* 8, 187.
- Wang, S., Wu, P.C., Su, V.-C., Lai, Y.-C., Chen, M.-K., Kuo, H.Y., Chen, B.H., Chen, Y.H., Huang, T.-T., Wang, J.-H., et al. (2018). A broadband achromatic metalens in the visible. *Nat. Nanotechnol.* 13, 227–232.
- Wang, S., Sun, X., Chen, D., Wang, S., Qi, Y., and Wu, F. (2020a). The investigation of height-dependent meta-lens and focusing properties. *Opt. Commun.* 460, 125129.
- Wang, W., Guo, C., Zhao, Z., Li, J., and Shi, Y. (2020b). Polarization multiplexing and bifocal optical vortex metalens. *Results Phys.* 17, 103033.
- Wang, Y., Wang, Z., Feng, X., Zhao, M., Zeng, C., He, G., Yang, Z., Zheng, Y., and Xia, J. (2020c). Dielectric metalens-based Hartmann-Shack array for a high-efficiency optical multiparameter detection system. *Photon. Res.* 8, 482–489.
- Wei, Y., Wang, Y., Feng, X., Xiao, S., Wang, Z., Hu, T., Hu, M., Song, J., Wegener, M., Zhao, M., et al. (2020). Compact optical polarization-insensitive zoom metalens doublet. *Adv. Opt. Mater.* 8, 2000142.
- West, P.R., Stewart, J.L., Kildishev, A.V., Shalaev, V.M., Shkunov, V.V., Strohkendl, F., Zakharenkov, Y.A., Dodds, R.K., and Byren, R. (2014). All-dielectric subwavelength metasurface focusing lens. *Opt. Express* 22, 26212–26221.
- Wilburn, B., Joshi, N., Vaish, V., Talvala, E.-V., Antunez, E., Barth, A., Adams, A., Horowitz, M., and Levoy, M. (2005). High performance imaging using large camera arrays. In *ACM SIGGRAPH 2005 Papers. ACM Trans. Graph.* 24, 765–776.
- Wildanger, D., Patton, B.R., Schill, H., Marseglia, L., Hadden, J.P., Knauer, S., Schönle, A., Rarity, J.G., O'Brien, J.L., Hell, S.W., et al. (2012). Solid immersion facilitates fluorescence microscopy with nanometer resolution and sub-ångström emitter localization. *Adv. Mater.* 24, OP309–OP313.
- Xie, X., Liu, K., Pu, M., Ma, X., Li, X., Guo, Y., Zhang, F., and Luo, X. (2019). All-metallic geometric metasurfaces for broadband and high-efficiency wavefront manipulation. *Nanophotonics* 9, 3209–3215.
- Xie, Y.-Y., Ni, P.-N., Wang, Q.-H., Kan, Q., Briere, G., Chen, P.-P., Zhao, Z.-Z., Delga, A., Ren, H.-R., Chen, H.-D., et al. (2020). Metasurface-integrated vertical cavity surface-emitting lasers for programmable directional lasing emissions. *Nat. Nanotechnol.* 15, 125–130.
- Xu, N., Liang, Y., Hao, Y., Mao, M., Guo, J., Liu, H., Meng, H., Wang, F., and Wei, Z. (2020). A thermal tuning meta-duplex-lens (MDL): design and characterization. *Nanomaterials* 10, 1135.
- Yan, C., Li, X., Pu, M., Zhang, F., Gao, P., Liu, K., and Luo, X. (2019). Midinfrared real-time polarization imaging with all-dielectric metasurfaces. *Appl. Phys. Lett.* 114, 161904.
- Yang, H., Li, G., Cao, G., Zhao, Z., Yu, F., Chen, X., and Lu, W. (2017). Polarization-independent metalens constructed of antennas without rotational invariance. *Opt. Lett.* 42, 3996–3999.
- Yang, J., Ghimire, I., Wu, P.C., Gurung, S., Arndt, C., Tsai, D.P., and Lee, H.W.H. (2019). Photonic crystal fiber metalens. *Nanophotonics* 8, 443–449.
- Ye, M., Ray, V., Wu, D., and Yi, Y.S. (2020). Metalens with artificial focus pattern. *IEEE Photon. Technol. Lett.* 32, 251–254.
- Yin, X., Steinle, T., Huang, L., Taubner, T., Wuttig, M., Zentgraf, T., and Giessen, H. (2017). Beam switching and bifocal zoom lensing using active plasmonic metasurfaces. *Light Sci. Appl.* 6, e17016.
- Yoon, G., Lee, D., Nam, K.T., and Rho, J. (2018). Geometric metasurface enabling polarization independent beam splitting. *Sci. Rep.* 8, 9468.
- Yoon, G., Jang, J., Mun, J., Nam, K.T., and Rho, J. (2019a). Metasurface zone plate for light manipulation in vectorial regime. *Commun. Phys.* 2, 156.
- Yoon, G., Kim, K., Kim, S.-U., Han, S., Lee, H., and Rho, J. (2021). Printable nanocomposite metalens for high-contrast near-infrared imaging. *ACS Nano* In press.
- Yoon, G., Kim, J., Mun, J., Lee, D., Nam, K.T., and Rho, J. (2019b). Wavelength-decoupled geometric metasurfaces by arbitrary dispersion control. *Commun. Phys.* 2, 129.
- Yoon, G., Kim, K., Huh, D., Lee, H., and Rho, J. (2020). Single-step manufacturing of hierarchical dielectric metalens in the visible. *Nat. Commun.* 11, 2268.
- Yu, N., and Capasso, F. (2014). Flat optics with designer metasurfaces. *Nat. Mater.* 13, 139–150.
- Yu, L., Fan, Y., Wang, Y., Zhang, C., Yang, W., Song, Q., and Xiao, S. (2020). Spin angular momentum controlled multifunctional all-dielectric metasurface doublet. *Laser Photon. Rev.* 14, 1900324.
- Yu, N., Genevet, P., Kats, M.A., Aieta, F., Tetienne, J.-P., Capasso, F., and Gaburro, Z. (2011). Light propagation with phase discontinuities: generalized laws of reflection and refraction. *Science* 334, 333–337.
- Yu, P., Li, J., Zhang, S., Jin, Z., Schütz, G., Qiu, C.-W., Hirscher, M., and Liu, N. (2018). Dynamic Janus metasurfaces in the visible spectral region. *Nano Lett.* 18, 4584–4589.
- Yuan, G., Rogers, K.S., Rogers, E.T.F., and Zheludev, N.I. (2019). Far-field superoscillatory metamaterial superlens. *Phys. Rev. Appl.* 11, 064016.
- Zhan, A., Colburn, S., Trivedi, R., Fryett, T.K., Dodson, C.M., and Majumdar, A. (2016). Low-contrast dielectric metasurface optics. *ACS Photon.* 3, 209–214.
- Zhang, C., Divitt, S., Fan, Q., Zhu, W., Agrawal, A., Lu, Y., Xu, T., and Lezec, H.J. (2020a). Low-loss metasurface optics down to the deep ultraviolet region. *Light Sci. Appl.* 9, 55.
- Zhang, F., Zeng, Q., Pu, M., Wang, Y., Guo, Y., Li, X., Ma, X., and Luo, X. (2020b). Broadband and high-efficiency accelerating beam generation by dielectric catenary metasurfaces. *Nanophotonics* 9, 2829–2837.

Zhang, J., Zhang, L., Huang, K., Duan, Z., and Zhao, F. (2019). Polarization-enabled tunable focusing by visible-light metasurfaces with geometric and propagation phase. *J. Opt.* 21, 115102.

Zheng, G., Mühlenbernd, H., Kenney, M., Li, G., Zentgraf, T., and Zhang, S. (2015). Metasurface holograms reaching 80% efficiency. *Nat. Nanotechnol.* 10, 308–312.

Zhou, H., Chen, L., Shen, F., Guo, K., and Guo, Z. (2019). Broadband achromatic metasurfaces in the midinfrared range. *Phys. Rev. Appl.* 11, 024066.

Zhou, Y., Kravchenko, I.I., Wang, H., Nolen, J.R., Gu, G., and Valentine, J. (2018). Multilayer noninteracting dielectric metasurfaces for multiwavelength metaoptics. *Nano Lett.* 18, 7529–7537.

Zhou, Y., Zheng, H., Kravchenko, I.I., and Valentine, J. (2020). Flat optics for image differentiation. *Nat. Photon.* 14, 316–323.

Zhu, A.Y., Chen, W.-T., Khorasaninejad, M., Oh, J., Zaidi, A., Mishra, I., Devlin, R.C., and Capasso, F. (2017). Ultra-compact visible

chiral spectrometer with meta-lenses. *APL Photon.* 2, 036103.

Zhu, A.Y., Chen, W.T., Sisler, J., Yousef, K.M.A., Lee, E., Huang, Y.-W., Qiu, C.-W., and Capasso, F. (2019). Compact aberration-corrected spectrometers in the visible using dispersion-tailored metasurfaces. *Adv. Opt. Mater.* 7, 1801144.

Zuo, R., Liu, W., Cheng, H., Chen, S., and Tian, J. (2018). Breaking the diffraction limit with radially polarized light based on dielectric metasurfaces. *Adv. Opt. Mater.* 6, 1800795.